Journal of Nuclear Materials 402 (2010) 38–54

Contents lists available at ScienceDirect

Journal of Nuclear Materials

journal homepage: www.elsevier.com/locate/jnucmat

Glass–ceramic nuclear waste forms obtained by crystallization of SiO_2–Al_2O_3–CaO–ZrO_2–TiO_2 glasses containing lanthanides (Ce, Nd, Eu, Gd, Yb) and actinides (Th): Study of the crystallization from the surface

P. Loiseau, D. Caurant *

Laboratoire de Chimie de la Matière Condensée de Paris (UMR CNRS 7574), Ecole Nationale Supérieure de Chimie de Paris (ENSCP, Chimie-ParisTech), 11 rue Pierre et Marie Curie, 75231 Paris, France

ARTICLE INFO

Article history:
Received 25 November 2009
Accepted 19 April 2010

ABSTRACT

Glass–ceramic materials containing zirconolite (nominally $CaZrTi_2O_7$) crystals in their bulk can be envisaged as potential waste forms for minor actinides (Np, Am, Cm) and Pu immobilization. In this study such matrices are synthesized by crystallization of SiO_2–Al_2O_3–CaO–ZrO_2–TiO_2 glasses containing lanthanides (Ce, Nd, Eu, Gd, Yb) and actinides (Th) as surrogates. A thin partially crystallized layer containing titanite and anorthite (nominally $CaTiSiO_5$ and $CaAl_2Si_2O_8$, respectively) growing from glass surface is also observed. The effect of the nature and concentration of surrogates on the structure, the microstructure and the composition of the crystals formed in the surface layer is presented in this paper. Titanite is the only crystalline phase able to significantly incorporate trivalent lanthanides whereas ThO_2 precipitates in the layer. The crystal growth thermal treatment duration (2–300 h) at high temperature (1050–1200 °C) is shown to strongly affect glass–ceramics microstructure. For the system studied in this paper, it appears that zirconolite is not thermodynamically stable in comparison with titanite growing form glass surface. Nevertheless, for kinetic reasons, such transformation (i.e. zirconolite disappearance to the benefit of titanite) is not expected to occur during interim storage and disposal of the glass–ceramic waste forms because their temperature will never exceed a few hundred degrees.

1. Zirconolite-based glass–ceramic materials as specific waste forms for actinides

Glass–ceramic materials (GCM) are composite materials constituted of a very high number of small crystals homogeneously dispersed in the bulk of a glassy matrix (the residual glass) that are generally produced by controlled crystallization of a parent glass of suitable composition following a two-stage thermal treatment (nucleation + crystal growth) [1–4]. Such kind of materials, and more particularly silicate based ones, are potential waste forms both for non-radioactive industrial wastes [5] – that can then find application in various fields such as building materials for instance – and for high level radioactive nuclear wastes (HLW) arising from the reprocessing of spent nuclear fuel. These radioactive wastes must be isolated from the biosphere for very long times until their radiotoxicity level drops back to a radiotoxicity level close to that of the initial uranium natural ores [6–9]. GCM are also envisaged for the immobilization of separated minor actinides [9], U-rich [10] and Pu-rich [11,12] wastes. GCM would benefit at the same time from the ease of glassy waste forms preparation by melting + casting and from the very good long term behavior and the high incorporation capacity of ceramic waste forms such as zirconates, titanates and phosphates. In the ideal case, GCM would consist of small and highly durable crystals (which would preferentially incorporate long-lived radionuclides such as actinides) homogeneously dispersed in a durable residual glass acting as a second barrier of containment for the radionuclides incorporated in the crystals (double containment principle). Due to the existence of a residual glassy phase embedding the crystals, such waste forms could accommodate more easily waste composition fluctuations and impurities than single phase ceramics. Indeed, because of the crystalline structure of ceramics, impurities and waste composition fluctuations could generate low durability parasitic phases containing radioactive elements.

GCM containing highly durable crystalline particles such as zirconolite (nominally $CaZrTi_2O_7$) homogeneously dispersed in the bulk of a glassy matrix and able to incorporate high quantities of actinides (such as minor actinides or Pu) or actinide surrogates (such as lanthanides) in their structure have been proposed as host candidates for the immobilization of these long-lived radionuclides [9,13,14]. In zirconolite ceramics it is known that actinides and their surrogates may be incorporated either into the Ca or Zr sites of the structure. For instance, more than 60% of the Ca^{2+} cations of

* Corresponding author. Tel.: +33 1 53737922; fax: +33 1 46347489.
E-mail address: daniel-caurant@chimie-paristech.fr (D. Caurant).

0022-3115/$ - see front matter © 2010 Elsevier B.V. All rights reserved.
doi:10.1016/j.jnucmat.2010.04.021

Zr-zirconolite can be replaced by Nd^{3+} or Gd^{3+} cations without changing the structure, following a charge compensation scheme with Al^{3+} cations into the titanium sites according to the following formula $Ca_{1-x}Nd_xZrTi_{2-x}Al_xO_7$ [15,16]. The choice of zirconolite as crystalline phase in the bulk of GCM is justified by the following reasons. Zirconolite is one of the best single phase ceramic that has been proposed as a host phase for the specific immobilization of separated minor actinides (Np, Am, Cm) or Pu by considering all its performances: high waste loading and chemical flexibility, excellent aqueous durability, good radiation resistance, existence of very old natural analogues [9,17–28]. Zirconolite was also envisaged in the SYNROC waste forms developed in Australia which consisted in an assemblage of three main thermodynamically compatible titanate crystalline phases (zirconolite + perovskite + hollandite) adapted for the immobilization of non-separated HLW (fission products + minor actinides) [29,30]. It is important to underline that despite the tendency of zirconolite to amorphize under alpha decay damages both in very old natural samples (containing U and Th) [31–34] and in artificial ceramic samples (containing for instance ^{244}Cm or ^{238}Pu) [28,35], it keeps a very high chemical durability in water. For instance, Lumpkin et al. [34] indicated that 550 million years old metamict zirconolite samples from Sri Lanka containing about 18 wt.% ThO_2 and 2 wt.% UO_2 showed only minor signs of geochemical alteration. Other studies reported in literature on zirconolite ceramic samples showed that the amorphization produced by external irradiation with heavy ions simulating α-recoils of actinides did not significantly affect the dissolution rate of zirconolite in water [21,36]. Chemical durability tests have also been performed in water on zirconolite ceramic samples under He^{2+} ions external irradiation – to simulate the effect of α-self-irradiation at the zirconolite/water interface – to study the impact of water radiolysis on the dissolution rate of zirconolite. It appeared that even under radiolytic conditions, zirconolite remained a good candidate for the specific immobilization of actinides [37,38]. This excellent chemical durability properties of zirconolite in water was explained by Leturcq et al. by considering the existence of a decalcified zirconolite phase on the surface of the altered zirconolite samples which would act as a passivation layer with protective properties [39]. The release of radiogenic helium during the annealing of amorphous Cm or Pu doped zirconolite ceramic samples was also studied and was associated with reordering and recrystallization phenomena [40].

In previous papers we showed that zirconolite-based GCM could be prepared either by nucleation + crystal growth of a Nd_2O_3 bearing (TiO_2, ZrO_2)-rich SiO_2–Al_2O_3–CaO parent glass [13,41–45] or by controlled cooling of the corresponding melt [14,46]. The possibility to replace partially or totally ZrO_2 by HfO_2 to prevent criticality events (hafnium has a high thermal neutron capture cross-section in comparison with zirconium) in the zirconolite crystals of these GCM was also studied [47]. In all these studies, neodymium was used as minor actinides surrogate. Nevertheless, it must be underlined that one of the drawbacks of these zirconolite-based GCM is that a significant fraction of actinides would probably remain in the residual glass surrounding the zirconolite crystals according to the results obtained using actinide surrogates [14]. Recently, Mahmoudysepehr et al. [48] also prepared zirconolite-based GCM for radioactive waste immobilization but from less refractory glass compositions belonging to the SiO_2–PbO–CaO–ZrO_2–TiO_2–B_2O_3–K_2O system (PbO, B_2O_3 and K_2O are known as good melting and fluxing agents during glass preparation). The chemical durability in water of zirconolite-based GCM prepared from (TiO_2, ZrO_2)-rich SiO_2–Al_2O_3–CaO parent glasses was studied at temperatures ranging from 50 to 200 °C in a mixed-flow hydrothermal reactor and it appeared that the initial dissolution rate r_0 of the GCM and of the corresponding parent glasses were similar but were an order of magnitude lower than that of borosilicate nuclear glasses and basaltic glasses [49–53]. However, lixiviation tests performed on high glass surface area (S) to solution volume (V) ratios ($S/V \approx 20{,}000\ m^{-1}$) in static alteration conditions at 90 °C that simulates more advanced degrees of reaction progress, showed that almost steady-state elementary normalized mass loss NL(Ca) were reached within a few days [49]. The GCM alteration rate $r(t)$ dropped by four orders of magnitude approaching zero ($r(t) < 10^{-5}$ g m^{-2} day^{-1}). According to these results [53], such a residual alteration rate would correspond to an alteration of roughly 3.6 μm in 10,000 years which is extremely small. This residual alteration rate value is lower than that of an inactive borosilicate nuclear glass ($r(t) < 10^{-4}$ g m^{-2} day^{-1}) but

Table 1
Nominal composition of lanthanide and thorium-doped parent glasses (in oxide weight and molar percentages). The composition of the parent glass G0 without actinide surrogate is also given.

Glass reference	Composition	SiO_2	Al_2O_3	CaO	TiO_2	ZrO_2	Ln_2O_3 or ThO_2	Na_2O
G0	wt.%	43.156	12.709	20.884	13.249	9.002	0.000	1.000
	mol%	48.848	8.477	26.328	11.282	4.968	0.000	1.097
GNd1	wt.%	42.724	12.582	20.675	13.117	8.912	1.000	0.990
	mol%	48.748	8.460	25.276	11.260	4.958	0.204	1.095
GNd2	wt.%	42.293	12.455	20.466	12.984	8.822	2.000	0.980
	mol%	46.647	8.442	25.223	11.236	4.948	0.411	1.093
GNd4	wt.%	41.430	12.201	20.049	12.719	8.642	4.000	0.960
	mol%	48.439	8.406	25.116	11.188	4.927	0.835	1.088
GNd6	wt.%	40.567	11.946	19.631	12.454	8.462	6.000	0.940
	mol%	48.226	8.369	25.005	11.138	4.905	1.274	1.083
GNd8	wt.%	39.703	11.692	19.213	12.189	8.282	8.000	0.920
	mol%	48.004	8.331	24.890	11.087	4.883	1.727	1.078
GNd10	wt.%	38.840	11.438	18.796	11.924	8.102	10.000	0.900
	mol%	47.774	8.291	24.772	11.034	4.859	2.196	1.073
GCe	wt.%	40.627	11.964	19.660	12.472	8.474	5.862	0.941
	mol%	48.226	8.369	25.005	11.138	4.905	1.274	1.083
GEu	wt.%	40.567	11.946	19.631	12.454	8.462	6.000	0.940
	mol%	48.253	8.373	25.019	11.145	4.908	1.218	1.084
GGd	wt.%	40.567	11.946	19.631	12.454	8.462	6.000	0.940
	mol%	48.270	8.376	25.028	11.149	4.910	1.183	1.084
GYb	wt.%	40.155	11.825	19.431	12.327	8.376	6.956	0.930
	mol%	48.226	8.369	25.005	11.138	4.905	1.274	1.083
GTh	wt.%	40.567	11.946	19.631	12.454	8.462	6.000	0.940
	mol%	48.058	8.340	24.918	11.099	4.888	1.617	1.080

higher than that of zirconolite ceramic ($r(t) < 10^{-6}$ g m^{-2} day^{-1}) using the same alteration conditions [49]. The quantity of altered materials varies in the same order as the residual alteration rate $r(t)$. For instance, according to Advocat et al. [49], after 200 days in static conditions at 90 °C, the normalized weight losses are the following for the different waste forms: inactive borosilicate nuclear glass (3×10^{-1} g m^{-2}) > zirconolite-based GCM (4×10^{-3} g m^{-2}) > zirconolite ceramic (1×10^{-3} g m^{-2}). Moreover, Martin et al. [50,51] showed that the long term release of actinide surrogates was mainly governed by the alteration of the residual glass remaining between zirconolite crystals in the bulk of the GCM (the zirconolite crystals being almost unaltered). More precisely, these authors showed that the initial alteration rate r_0 was controlled by the preferential alteration of the residual glass around zirconolite crystals that induced an increase of the accessible glass + crystals surface area. Consequently, among the three source terms for actinides release, one for the zirconolite crystals, one for the residual glass and one for the grain boundary, the last one being the most rapid, it will govern the overall release of actinides. In comparison with nuclear borosilicate glasses, the higher chemical durability of zirconolite-based GCM can be explained by the occurrence of ZrO_2 and TiO_2, the lack of boron and the very small amount of sodium in glass (see Table 1 below). The initial alteration step is followed by the formation of alteration films on the residual glass and crystals surface that induces a high slowdown of the alteration rate because these films act as diffusive barriers (protective effect) [53]. Recent studies [54,55] coupling experimental results on silicate glasses corrosion with numerical Monte Carlo simulations showed the strong impact of morphological transformations in the altered layer on leaching kinetics: the sharp drop of alteration rate was shown to arise from densification of the outer layers of the film (porosity closure).

2. Previous studies on the crystallization of zirconolite-based glass–ceramic materials

The comparison of the different methods that have been used to prepare Nd-doped zirconolite-based GCM in our previous studies either from the glass or from the melt [14,46], clearly indicates that the occurrence of titanite (nominally $CaTiSiO_5$) and anorthite (nominally $CaAl_2Si_2O_8$) crystals from sample surface can compete with the crystallization of zirconolite in the bulk (Fig. 1). Only these two silicate phases nucleate heterogeneously on glass surface and form a partially crystallized layer that grows towards the bulk of glass samples. The origin of surface induced crystallization in glasses was discussed for instance in [56]. The evolution with the heating temperature of the nature of the main crystalline phases formed in the bulk and near the surface of the Nd-doped zirconolite-based GCM is summarized in Fig. 1. The thickness of the titanite + anorthite layer never exceeds 1 mm as shown in Fig. 2 and is easy to control by using a nucleation (2 h at 810 °C) + crystal growth (2 h between 1000 °C and 1200 °C) method [14,46]. This last crystallization method corresponds to the classical one used to prepare glass–ceramics in industry [1]. Moreover, the activation energy associated with the crystal growth of titanite and anorthite was determined using differential thermal analysis (DTA) methods and the evolution of the exothermic effects associated with the crystallization of these two phases was followed according to the glass particle sizes [57]. It is worth noting that titanite-based GCM – prepared from parent glasses belonging to the system SiO_2–Al_2O_3–CaO–Na_2O–TiO_2 – were extensively studied and envisaged in the 1980s by Canadian researchers as candidate waste forms for the immobilization of CANDU fuel wastes [58,59]. In this case, the titanite phase was also observed to nucleate preferentially heterogeneously on external surfaces and on internal heterogeneities. It is also worth noting that because titanite is a phase present in a wide range of igneous rocks, several studies have been reported in literature on the distribution of high field strength elements such as lanthanides, zirconium and thorium (present as trace elements) between titanite and silicate melts [60]. Because titanite has a relatively high capacity to incorporate lanthanides, its crystallization in rocks may significantly affect their distribution. Moreover, studies have been performed on the effect of the nature and concentration of lanthanides in silicate melts on the partition coefficient D of lanthanides between titanite and the melt [60–63]. The impact of silicate melt composition – and more particularly of the amount of Al_2O_3 and non-bridging oxygens – on D was also studied [60,61].

In a previous paper [13], we studied the controlled crystallization in the bulk of a parent glass composition belonging to the SiO_2–Al_2O_3–CaO–ZrO_2–TiO_2 system containing minor actinide and Pu surrogates such as Ce, Nd, Eu, Gd, Yb and Th. The choice of these different surrogates was discussed in [13]. In all cases, zirconolite was shown to be the only crystalline phase able to nucleate directly in the bulk of the GCM. This result can be explained by the well known strong tendency of Ti^{4+} and Zr^{4+} ions to act as very efficient nucleating agents in glasses due to their high field

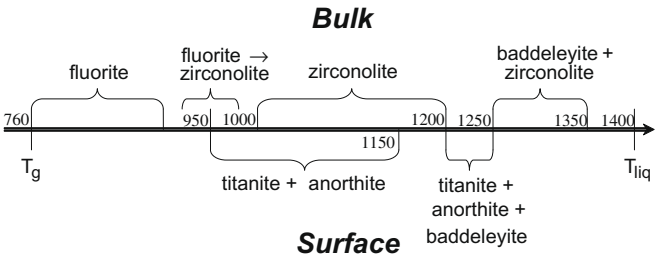

Fig. 1. Evolution with the thermal treatment temperature T_c (950–1350 °C) of the nature of the main crystalline phases formed in the bulk (fluorine, zirconolite, baddeleyite) or near the surface (titanite, anorthite, baddeleyite) of the Nd-bearing zirconolite-based GNd6 GCM. This figure summarizes the main results presented in [14,41–43,46]. T_g and T_{liq} are respectively the glass transformation temperature and the liquidus temperature of the GNd6 parent glass. The fluorite phase formed in the bulk for $T_c < 1000$ °C is in a fact a cubic defect-fluorite phase that transforms irreversibly into zirconolite for $T_c \geqslant 1000$ °C [43].

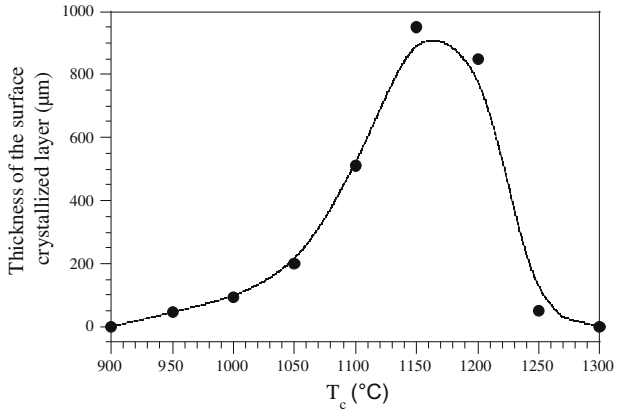

Fig. 2. Evolution with crystal growth temperature (T_c) of the thickness of the crystallized layer – mainly constituted of titanite and anorthite crystals (see Fig. 3) – growing from the GCM surface towards the bulk of the Nd-doped sample (GNd6). The parent glass was previously nucleated during 2 h at 810 °C to induce crystallization of zirconolite in the bulk [13,41]. It can be noticed that the crystallized layer is only observed when 950 °C $\leqslant T_c \leqslant$ 1250 °C. For $T_c \leqslant 900$ °C, titanite and anorthite crystal growth kinetics become to low whereas for $T_c \geqslant 1300$ °C, these two phases are not ever stable in the supercooled melt. This last point is in agreement with previous DTA results which showed that during heating, these two phases dissolved in the melt near 1260–1270 °C [57].

strength and thus to their tendency to separate from the silicate network forming for instance very small (Zr, Ti)-rich crystallites able to induce the heterogeneous nucleation of the remaining supercooled liquid on their surface and thus in the bulk of the glass (volume nucleation) [1,64–69]. The effect of the nature of the actinide surrogate on the structure, the microstructure and the composition of the zirconolite crystals formed in the bulk of the GCM was widely studied in [13]. A correlation was observed between surrogate cations field strength in the glass and zirconolite nucleation rate. The amount of lanthanides and thorium incorporated into zirconolite crystals was discussed in relation with the capacity of the glass to accommodate these elements (in accordance with their cationic field strength) and with the capacity of the crystals to incorporate them in the calcium and zirconium sites of their structure (bond valence–bond length considerations [70,71] were used to quantify the ability of the calcium and zirconium sites of the zirconolite structure to accept lanthanide and Th^{4+} ions).

In the present paper, we study the effect of the nature of minor actinide and Pu surrogates (Ce, Nd, Eu, Gd, Yb, Th) on the crystallization processes occurring from the surface of SiO_2–Al_2O_3–CaO–ZrO_2–TiO_2 glasses. The nature, the structure, the microstructure and the composition of the crystalline phases nucleating and growing from the GCM surface are presented and the amount of surrogates incorporated in their structure is determined. The effect of the duration of the crystal growth thermal treatment from 2 to 300 h at 1050 °C and 1200 °C on the stability of the zirconolite crystals formed initially in the bulk of parent glasses in competition with the silicate phases growing from glass surface is studied for the Nd-, Eu-, Gd-, and Th-doped samples and for a sample without actinide surrogate. Concerning more specially the neodymium-doped parent glass, the effect of Nd_2O_3 concentration (from 0 to 10 wt.%) on both the structure and the composition of the crystalline phases growing from the surface is also presented.

3. Experimental procedures

The compositions of the lanthanide and thorium-doped parent glasses prepared for this study are given in Table 1 and were initially chosen to study the crystallization of zirconolite in the bulk of the samples [13,72]. For each actinide surrogate, the same basic undoped parent glass composition G0 was used [41] (in wt.%): SiO_2 (43.16), Al_2O_3 (12.71), CaO (20.88), TiO_2 (13.25), ZrO_2 (9.00), Na_2O (1.00). The doped glasses were prepared with the following simulant levels (wt.%): Ce_2O_3 (5.86), Nd_2O_3 (1.00 to 10.00), Eu_2O_3 (6.00), Gd_2O_3 (6.00), Yb_2O_3 (6.95), ThO_2 (6.00). The Ce_2O_3, Eu_2O_3, Gd_2O_3 and Yb_2O_3 molar concentrations for all the samples (Table 1) are approximately similar to the one of the 6 wt.% Nd_2O_3 doped glass (GNd6). This composition was widely studied in [41] and corresponds approximately to a 9.2 wt.% Am_2O_3-doped glass which is close to the amount of minor actinides aimed to be incorporated in the waste form (≈10 wt.%). However, because of the high atomic weight of thorium, Th molar concentration in glass GTh is close to that of Nd in glass GNd4 (Table 1). All glasses (≈40 g) were prepared after thorough mixing of reagent grade oxide (SiO_2, Al_2O_3, ZrO_2, TiO_2, CeO_2, Nd_2O_3, Eu_2O_3, Gd_2O_3, Yb_2O_3, ThO_2) and carbonate ($CaCO_3$, Na_2CO_3) powders. The preparation method and the coloration of parent glasses obtained were already described in [13]. The GCM samples (cylinders of 1 cm diameter and 1 cm high) were then prepared by a two-step thermal treatment of parent glasses including a 2 h nucleation stage at T_n = 810 °C and a 2 h crystal growth stage at either T_c = 1050 °C or 1200 °C before annealing at 755 °C. Nucleation temperature was kept constant for all glass samples because the parent glass transformation temperature T_g (≈760 °C) does not significantly change between the different compositions studied. Indeed, the temperature range where zirconolite nucleation is significant was shown to be located only slightly higher than T_g [42]. The two crystal growth temperatures chosen in this study (T_c = 1050 °C and 1200 °C) were shown to lead to the crystallization of zirconolite as the only crystalline phase in the bulk of the Nd-doped glasses [41]. For the neodymium-doped glass (GNd6) and for a 2 h thermal treatment, the effect of the crystal growth temperature T_c from 900 °C to 1300 °C on the thickness of the surface crystallized layer was determined (Fig. 2).

In order to study the competition between the zirconolite crystals formed in the bulk and the silicate crystallized layer growing from the surface towards the bulk of the glass, the duration of the crystal growth thermal treatment at T_c = 1050 °C and 1200 °C was increased from 2 h to 20 h for the GNd6, GEu, GGd, GTh and G0 samples. For the GNd6 glass, a GCM sample was also prepared at 1050 °C for 300 h.

In order to complete this work, three neodymium-doped ceramic samples were also prepared:

- A zirconolite ceramic ($Ca_{0.7}Nd_{0.3}ZrTi_{1.7}Al_{0.3}O_7$) using the preparation method given in [13].
- A titanite ceramic ($Ca_{0.88}Nd_{0.12}Ti_{0.70}Zr_{0.18}Al_{0.12}Si_{1.00}O_5$) synthesized at 1300 °C by solid state reaction from reagent grade oxide and carbonate powders.
- A neodymium silicate apatite + cristobalite mixture corresponding to the molar composition $8SiO_2$–$4CaO$–$1Nd_2O_3$ prepared by solid state reaction from reagent grade oxide and carbonate powders (1400 °C for 25 h + 1500 °C for 25 h).

All the GCM samples were characterized by X-ray diffraction (XRD) using a Siemens D5000 apparatus operating at CoK_α wavelength (λ = 1.778897 Å). The bulk and the crystallized surface layer of GCM were studied by scanning electron microscopy (SEM) and energy dispersive X-ray analysis (EDX) using polished and carbon coated samples with a Hitachi S2500 microscope equipped with a PGT analyzer (accelerating voltage 15 kV, beam current ≈ 1.8 nA). For each GCM sample, the corresponding parent glass was used as reference for the determination of crystals and residual glass composition by EDX. Such analysis were only performed for the GCM samples prepared at T_c = 1200 °C for which crystals were large enough to be probed by the microscope electron beam both in the crystallized layer and in the bulk. A least six measurements were performed and averaged for each phase and each sample.

Magnetic and optical properties of Nd^{3+} ions were used to get information about the evolution of their local environment in the GCM after short (2 h) and long (300 h) heat treatment durations at 1050 °C.

Electron spin resonance (ESR) experiments were performed at 12 K on the Nd-doped titanite and zirconolite ceramics and on several glass and GCM samples (GNd6) in order to follow the incorporation of the Nd^{3+} paramagnetic ions in the different phases occurring after crystallization with the help of a Bruker ESP 300e spectrometer operating at X-band ($\nu \approx 9.5$ GHz). The necessity to record the ESR spectra at low temperature is due to the very short spin–lattice relaxation time T_1 of Nd^{3+} ions associated with their strong spin–orbit coupling constant. As the samples studied here are not single crystals, the ESR spectra recorded are relatively wide (generally more than 9000 G) and correspond to more or less defined powder spectra. However, their shape is characteristic of the local environment around neodymium ions.

Optical absorption spectra corresponding to the electronic transition between the $^4I_{9/2}$ ground state manifold and the excited state $^2P_{1/2}$ manifold were recorded at low temperature (T < 15 K) for the same samples (200 mg KBr pellets containing 25 wt.% of Nd-doped material) using a Varian Cary 5E double beam spectrometer. The $^4I_{9/2} \rightarrow {}^2P_{1/2}$ transition is interesting because the degeneracy of

the $^2P_{1/2}$ state is not removed by the crystal field occurring around Nd^{3+} ions. However, the $^4I_{9/2}$ ground state manifold is, at the most, decomposed by the crystal field (due to the effect of the immediate environment of the Nd^{3+} ions, i.e. their first coordination shell consisting of oxygen anions) into five Stark levels. But only the one of lowest energy is populated at low temperature. Thus, at low temperature, each kind of neodymium environment in the GCM is characterized by only one $^4I_{9/2} \rightarrow {}^2P_{1/2}$ absorption band on the spectra whose position both depends on the Nd–O bond covalency (nephelauxetic effect) and on the local crystal field around neodymium [73].

4. Results and discussion

4.1. Effect of the nature of the actinide surrogate on the nature, the microstructure and the structure of the crystals growing from glass–ceramic surface

For the G0, GCe, GNd6, GEu, GGd and GYb GCM prepared at T_c = 1050 °C or 1200 °C, a thin crystallized layer consisting mainly of titanite and anorthite crystals is observed by SEM (Fig. 3). For all these samples, the layer thickness increases from 170 to 190 μm to 500 to 1000 μm at T_c ranging respectively from 1050 °C to 1200 °C (see Fig. 2 for the GNd6 sample). The evolution of the layer thickness with temperature can be explained both by:

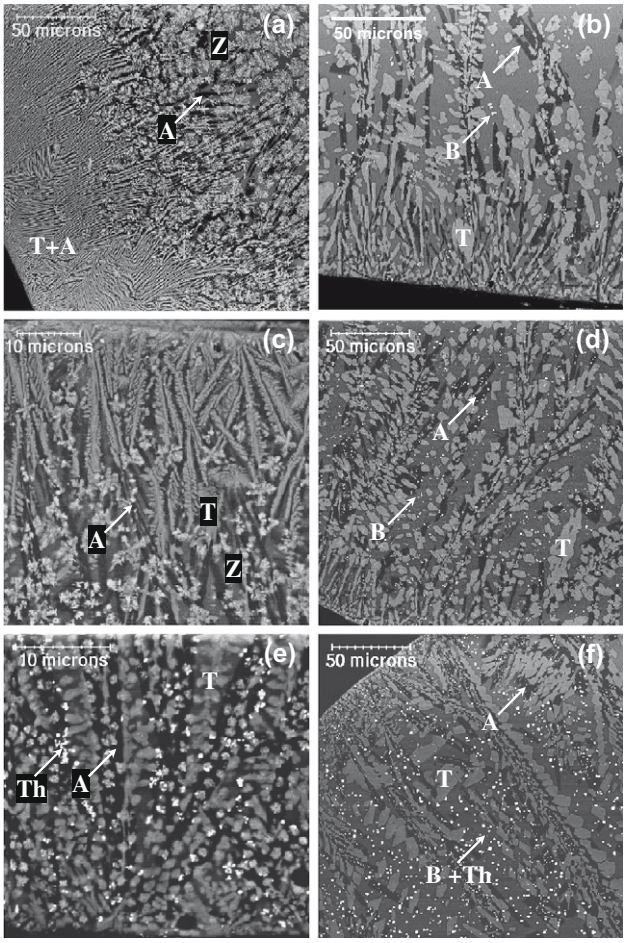

Fig. 3. Back-scattered SEM images of the crystallized layer formed in the Nd- (a, b), Gd- (c, d) and Th- (e, f) doped GCM prepared at T_c = 1050 °C (a, c, e) and 1200 °C (b, d, f). Titanite appears as grey crystals whereas anorthite crystals are darker than the residual glass. Due to the high molecular weight of Zr and Th, baddeleyite and thoria appear as white crystals on the images. T: titanite, A: anorthite, B: baddeleyite, Th: thoria.

- The decrease of the titanite + anorthite crystal growth kinetics barrier when T_c increases due to the decrease of the supercooled melt viscosity.
- The decrease of the titanite + anorthite crystallization driving force when T_c increases.
- The evolution of the microstructure of the zirconolite crystals in the bulk [13] which can strongly disturb the growth of the surface layer growing at 1050 °C.

For T_c = 1200 °C, small baddeleyite (nominally ZrO_2) crystals are also observed among the silicate phases for all the samples (Fig. 3b, d). Concerning the thorium-doped GTh GCM, the same surface crystalline phases as previously are also formed excepted that a large amount of thoria (nominally ThO_2) crystallization is also detected between the silicate crystals at the two crystal growth temperatures (Fig. 3e, f). For this sample, the crystallized layer thickness increases from 190 μm to 500 μm at T_c ranging respectively from 1050 °C to 1200 °C. For the lanthanide-doped samples prepared at T_c = 1050 °C (Fig. 3a, c), the microstructure of the layer consists of a high density of elongated dendritic titanite crystals and of needle-shape anorthite crystals. All these crystals nucleate on the glass surface and then grow towards the bulk of the GCM. This leads to a very anisotropic microstructure contrary to the crystallization of zirconolite in the bulk of the glass [13]. For T_c = 1200 °C, the crystals are thicker (Fig. 3b, d, f) and can be easily probed by the electron beam of EDX analysis (see below). The comparison of the SEM images of the crystallized layer with that corresponding to the bulk reported in [13] shows that the amount of crystalline phases is higher near the surface than in the bulk of GCM (see also Fig. 11g, i below). Indeed, the volume percentage of the different phases constituting the partially crystallized layer was estimated by SEM image analysis for the GNd6 sample heat treated at T_c = 1200 °C: residual glass (51%), titanite (31%), anorthite (17%), baddeleyite (1%) whereas the amount of residual glass in the bulk for this same sample represented approximately 90% (≈10 vol.% zirconolite). This strong difference of crystallinity between the surface and the bulk is due to the fact that zirconolite crystals do not consume silica – which is the main oxide in the parent glass composition (see Table 1) – during their growth contrary to both titanite and anorthite crystals. This result was confirmed by XRD in [41].

4.2. Effect of the nature of the actinide surrogate on the composition of the crystals formed near the surface of the glass–ceramics

The composition of the titanite crystals formed near the surface of the GCM was determined by EDX for all the samples heat treated at 1200 °C (Table 2, Fig. 4). For several samples, the composition of the baddeleyite (ZrO_2) and anorthite crystals is also reported in Table 2. The composition of the residual glass remaining between the crystals of the crystallized layer formed at 1200 °C is given in Table 3 and in Figs. 5 and 6 for several samples.

It appears that for all the GCM (doped or not with surrogates), lanthanide, thorium, titanium and zirconium ions do not enter into the anorthite crystals. The fact that anorthite has a totally polymerized tri-dimensional structure constituted of SiO_4 and AlO_4 tetrahedra [74] without non-bridging oxygen atoms could explain the difficulty to incorporate significant amounts of actinide surrogate in this phase. Moreover, the fact that heavy elements are not incorporated into anorthite explains why this phase appears as black crystals on the SEM images (Fig. 3). Consequently, this phase is not expected to incorporate neither minor actinides nor plutonium in the GCM. However in all cases, approximately 20% of the calcium sites of the anorthite nominal composition ($CaAl_2Si_2O_8$) are occupied by sodium ions. Thus, this silicate phase is not purely anorthite but belongs to the anorthite ($CaAl_2Si_2O_8$) – albite (NaAl-

Table 2
Compositions determined by EDX for the titanite, baddeleyite and anorthite crystals formed in the surface crystallized layer at T_c = 1200 °C. For all the lanthanides (except Ce), the oxidation state was assumed to be trivalent in titanite crystals. For cerium, two compositions are given for titanite, assuming only Ce^{3+} or a Ce^{3+}/Ce^{4+} mixture in the structure. Titanium was assumed to occur only as Ti^{4+} in all crystals. /: composition not determined, □: calcium vacancy.

Sample reference	Titanite	Baddeleyite	Anorthite
GCe	$Ca_{0.92}Ce^{3+}_{0.07}Ti_{0.77}Zr_{0.22}Al_{0.09}Si_{0.93}O_5$ or $Ca_{0.93}Ce^{3+}_{0.05}Ce^{4+}_{0.02}Ti_{0.77}Zr_{0.21}Al_{0.09}Si_{0.93}O_5$	$Zr_{0.85\pm0.02}Ce^{4+}_{0.08\pm0.02}Ti_{0.07}O_2$	/
GNd6	$Ca_{0.89}Nd_{0.11}Ti_{0.69}Zr_{0.22}Al_{0.11}Si_{0.98}O_5$	$Zr_{0.93}Ti_{0.07}O_2$	$Ca_{0.77}Na_{0.19}\square_{0.04}Al_{1.73}Si_{2.27}O_8$
GEu	$Ca_{0.89}Eu_{0.10}Ti_{0.73}Zr_{0.20}Al_{0.12}Si_{0.96}O_5$	/	/
GGd	$Ca_{0.88}Gd_{0.12}Ti_{0.73}Zr_{0.22}Al_{0.12}Si_{0.93}O_5$	$Zr_{0.93}Ti_{0.06}Gd_{0.01}O_{1.995}$	/
GYb	$Ca_{0.92}Yb_{0.06}Ti_{0.74}Zr_{0.21}Al_{0.10}Si_{0.97}O_5$	/	/
GTh	$Ca_{0.97}Th_{0.02}Ti_{0.78}Zr_{0.22}Al_{0.06}Si_{0.95}O_5$	$Zr_{0.90}Ti_{0.08}Th_{0.02}O_2$	/
G0	$Ca_{0.99}Ti_{0.78}Zr_{0.23}Al_{0.02}Si_{0.98}O_5$	/	$Ca_{0.78}Na_{0.17}\square_{0.05}Al_{1.73}Si_{2.27}O_8$

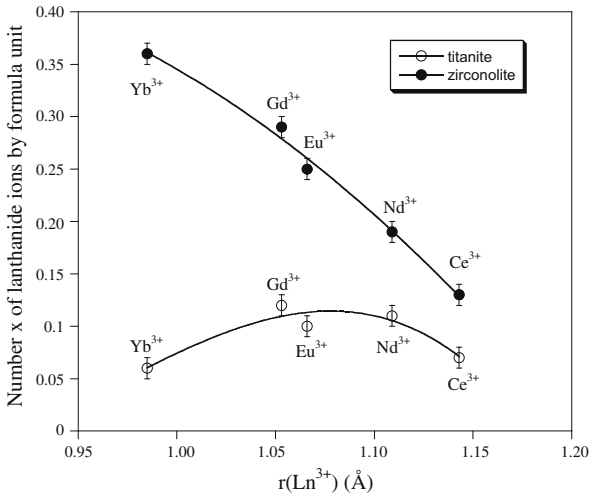

Fig. 4. Evolution as a function of the Ln^{3+} cation radius (in 8-fold coordination [82]) of the number x of lanthanide ions incorporated by formula unit in the titanite crystals formed in the layer near the GCM surface at T_c = 1200° C (2 h) (see Tables 2 and 4) and of the number x of lanthanide ions by formula unit incorporated in the zirconolite crystals formed in the bulk of the GCM at T_c = 1200° C (2 h) (see Table 4 in [13]).

Si_3O_8) solid solution series [75]. However, for practical reasons, we will continue to use the name anorthite for this phase in this paper. It is interesting to note that this phase is the only crystalline phase that incorporates Na^+ ions in the GCM studied in this work (Table 2). As in anorthite nominal composition there is one Ca site by formula unit, we assumed the existence of vacancies in this site: $Ca_{0.77}Na_{0.19}\square_{0.04}Al_{1.73}Si_{2.27}O_8$ (where □ represents calcium vacancies). However, due to the well known difficulties to analyze precisely sodium in materials by EDX [76], the true sodium concentration in anorthite crystals is probably underestimated in our analysis. Taking this into account, it is probably not necessary to assume the existence of calcium vacancies and a more realistic composition of anorthite crystals could be: $Ca_{0.75}Na_{0.25}Al_{1.75}Si_{2.25}O_8$.

Table 2 also indicates that neither lanthanides nor thorium ions enter significantly into the baddeleyite (ZrO_2) crystals. For Th, this result is not surprising because ThO_2 solubility is known to be very low in ZrO_2 [77]. However, all trivalent lanthanide ions are known to be able to substitute for Zr^{4+} ions in ZrO_2 creating oxygen vacancies in the zirconia structure [77]. This charge compensation process is probably not efficient in our samples which could explain the lack of trivalent lanthanide ions incorporation in the baddeleyite crystals (Table 2). Nevertheless, for the Ce-doped sample, a low but significant amount of cerium was incorporated in the baddeleyite crystals. This can be understood if we consider that all the cerium ions in the baddeleyite crystals are in tetravalent state. Indeed, contrary to ThO_2, literature indicates that approximately 20 mol% CeO_2 is able to make solid solution with ZrO_2 [77]. In this case, Ce^{4+} ions directly replace Zr^{4+} ions in the zirconia structure. The occurrence of tetravalent cerium ions in the crystallized layer near sample surface could be due to the displacement of $Ce^{3+} \leftrightarrow Ce^{4+}$ equilibrium towards oxidation during the crystal growth thermal treatment at T_c = 1200 °C (it must be recalled that

Table 3
Composition determined by EDX of lanthanide and thorium-doped residual glass in the surface crystallized layer formed after 2 h heat treatment at T_c = 1200 °C (in oxide weight and molar percentages). The composition of the residual glass for the sample G0 without actinide surrogate is also given.

Surface residual glass	Composition	SiO_2	Al_2O_3	CaO	TiO_2	ZrO_2	Ln_2O_3 or ThO_2	Na_2O
G0	wt.%	56.21	14.08	19.30	4.85	4.28	0.000	1.28
	mol%	60.99	9.00	22.44	3.96	2.26	0.000	1.35
GNd1	wt.%	56.38	13.66	19.25	4.46	4.11	0.62	1.52
	mol%	61.28	8.75	22.42	3.65	2.18	0.12	1.60
GNd2	wt.%	55.02	13.72	18.91	4.53	4.26	1.73	1.83
	mol%	60.50	8.89	22.28	3.75	2.28	0.34	1.95
GNd6	wt.%	51.51	12.96	18.25	4.97	4.33	6.67	1.28
	mol%	59.21	8.78	22.48	4.30	2.43	1.37	1.43
GNd10	wt.%	47.23	11.88	17.77	5.03	4.62	11.97	1.47
	mol%	56.98	8.45	22.98	4.57	2.72	2.58	1.72
GCe	wt.%	48.03	13.83	19.30	5.90	4.49	6.90	1.54
	mol%	55.69	9.45	23.98	5.15	2.54	1.47	1.73
GEu	wt.%	51.46	13.70	19.07	4.80	3.77	5.82	1.37
	mol%	58.65	9.20	23.29	4.11	2.09	1.13	1.51
GGd	wt.%	50.17	16.23	17.88	4.08	4.34	5.55	1.74
	mol%	57.88	11.04	22.10	3.54	2.44	1.06	1.95
GYb	wt.%	50.31	12.87	19.51	5.18	4.74	6.38	1.00
	mol%	57.86	8.72	24.04	4.48	2.66	1.12	1.12
GTh	wt.%	49.16	13.33	18.41	5.55	4.44	7.70	1.40
	mol%	57.04	9.11	22.88	4.84	2.51	2.03	1.57

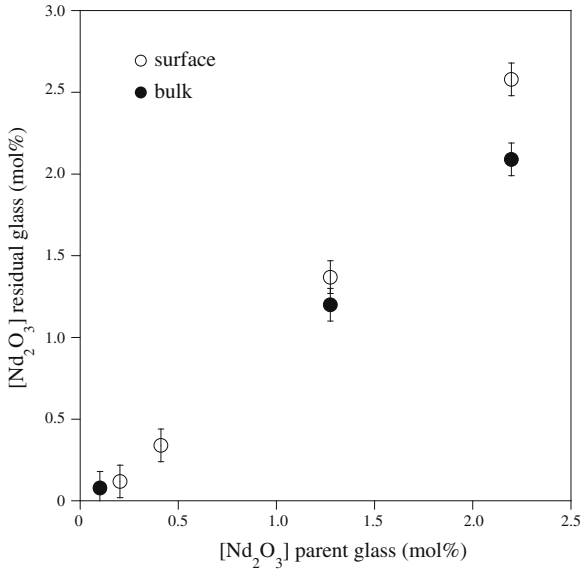

Fig. 5. Evolution of Nd_2O_3 content (mol%) in the residual glass of the partially crystallized surface layer (T_c = 1200 °C, 2 h) versus Nd_2O_3 content in the corresponding Nd-bearing parent glass.

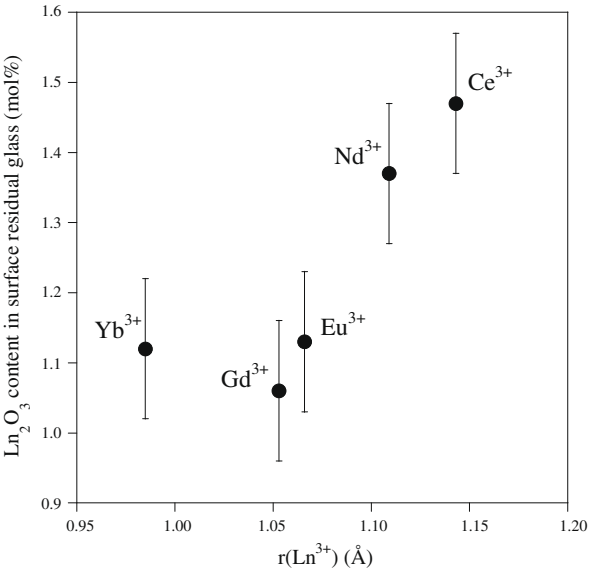

Fig. 6. Evolution of Ln_2O_3 content (mol%) in the residual glass of the partially crystallized surface layer (T_c = 1200 °C, 2 h) as a function of the Ln^{3+} cation radius (in 8-fold coordination [82]) for GNd6, GCe, GEu, GGd and GYb samples.

the cerium-doped parent glass GCe was prepared at 1650 °C in order to strongly increase the amount of Ce^{3+} ions [13]).

Concerning titanite crystals, the results reported in Table 2 show that this crystalline phase is the only one able to incorporate trivalent lanthanide ions (Ln^{3+}) in the surface crystallized layer. It appears that Ln^{3+} ions are only incorporated into the calcium site of the titanite structure (there is only one type of calcium site in this structure and this site is 7-fold coordinated with oxygen ions [78]) probably because the tetrahedral silicon and the octahedral titanium sites are too small. This result is in accordance with the one published by Higgins et al. for natural titanite samples [79]. In our GCM, the positive charge excess due to Ln^{3+} ions incorporation in the calcium site of titanite is compensated by the simultaneous incorporation of Al^{3+} ions probably both in the titanium and silicon sites (Table 2). It is interesting to underline that for our GCM, the amount of Ln^{3+} ions incorporated in the Ca site always remains lower than the solubility limit (20 mol%) reported in the literature for La^{3+} ions in titanite ceramic following $Ca_{1-x}La_xTi_{1-x}Al_xSiO_5$ incorporation scheme [80]. The preferential incorporation of lanthanide ions in the titanite Ca site was also observed by Hayward [58,59] in the titanite-based GCM that were developed for CANDU waste immobilization. In this case, the trivalent lanthanide cations introduced in the parent glass composition entered into the titanite calcium site following $Ca_{1-x}Ln_xTi_{1-x}Al_xSiO_5$ or $Ca_{1-x}Ln_{x/2}Na_{x/2}TiSiO_5$ incorporation schemes [59]. The occurrence of this last charge balance scheme to incorporate lanthanide ions simultaneously with sodium ions could be due to a higher Na_2O content (5–9 wt.%) in the Canadian GCM than in our samples (1 wt.%). It is worth noting that in their works on the partitioning of trace elements between titanite and silicate melts, Prowatke et al. [60,61] suggested that at trace levels, lanthanides may be incorporated in titanite structure partly by coupled substitution with Ca vacancies. Nevertheless, these authors [60] underlined the fact that different substitution mechanisms may operate in titanite for trace elements and for major elements with a coupled substitution mechanism of lanthanides in Ca site with Al in Ti site when lanthanides are major elements as reported by Green et al. [62]. However, it is interesting to remark that the convex-upward shape of the curve showing the evolution of the titanite–silicate melt partition coefficient versus lanthanide ionic radius given by Prowatke et al. [60,61] is similar to that given in Fig. 4 showing the evolution in our GCM of the number x of lanthanide ions incorporated by formula unit in the titanite crystals versus lanthanide ionic radius. Indeed, in both studies, titanite crystals accommodated more readily the middle lanthanides (close to Gd) than the light (Ce) or the heavier (Yb) lanthanides.

It is interesting to compare, in our GCM prepared at T_c = 1200 °C, the lanthanide incorporation level by formula unit in titanite (surface) with the one of zirconolite (bulk) (Fig. 4). It clearly appears that the zirconolite crystals are more efficient to incorporate the actinide surrogates than the titanite crystals formed near samples surface. This is in accordance with the Ln^{3+} solubility limits reported in literature both for titanite [80] and zirconolite [15,16] ceramic samples. This difference of behavior concerning lanthanide incorporation between the two phases could be partly explained by the fact that in zirconolite there are two sites (the Ca and Zr ones) able to accept substitution by Ln^{3+} ions. In [13] we showed that in our GCM, the Zr site in zirconolite was able to incorporate relatively high amounts of the smallest lanthanide of the series (Yb). This remark is in accordance with the increasing difference observed in Fig. 4 between the two curves when Ln^{3+} radius decreases.

The comparison of the composition of the residual glass remaining between the crystals of the surface layer (T_c = 1200 °C, Table 3) with that of parent glass for the Nd-doped GNd6 sample (Table 1) shows important differences. For instance, for the residual glass composition, we observe:

- A strong decrease of TiO_2 concentration that can be mainly attributed to the high volume percentage of titanite formed in the layer (31 vol.% for GNd6 sample).
- A decrease of ZrO_2 concentration due both to baddeleyite (ZrO_2) crystallization and to the incorporation of zirconium in titanite (Table 2).
- An increase of SiO_2 concentration which can be explained by the fact that the silica molar concentration in titanite (33 mol% at the most) is lower than that of the parent glass (48.2 mol%) whereas it is only slightly increased in anorthite (50 mol%).
- The amount of Nd_2O_3 is slightly higher in the residual glass (Table 3, Fig. 5) than in parent glass (Table 1). This result can

be explained both by the limited amount of Nd incorporated in titanite and by the lack of Nd incorporation in anorthite (Table 2). For comparison, the amount of Nd_2O_3 in the residual glass of the bulk between the zirconolite crystals formed at T_c = 1200 °C is also reported in Fig. 5. It appears that Nd_2O_3 concentration is slightly higher in the residual glass near the surface than in the bulk.

Concerning thorium, EDX results show that only a very low amount of Th^{4+} ions (0.02 ions by formula unit) is detected in titanite crystals at T_c = 1200 °C (Table 2). Nevertheless as this thorium concentration is below the EDX detection limit (about 1 atom%), so as there may be no significant amount of thorium in the titanite crystals. This result could be explained by the very low solubility limit ($x \approx 0.03$–0.05) of ThO_2 in titanite following the incorporation scheme $Ca_{1-x}Th_xTi_{1-2x}Al_{2x}SiO_5$ [80]. Our result is also in agreement with that of Prowatke et al. [60] which showed that the titanite–silicate melt partitioning coefficient for Th was lower than for lanthanides by about two orders of magnitude. However, these authors also showed that, as for lanthanides, Th partitioning between titanite crystals and silicate melt strongly increased with Al_2O_3 content in parent glass. Once again, it appears that in our GCM, titanite crystals are less efficient than zirconolite ones to incorporate actinide surrogates in their structure. It can be reminded that at T_c = 1200 °C, the composition of the zirconolite crystals formed in the bulk of the GTh sample was the following: $Ca_{0.90}Th_{0.09}Zr_{1.04}Ti_{1.77}Al_{0.20}O_7$ [13]. Moreover, in this case the crystallization of thoria was not observed in the bulk. The fact that none of the crystalline phases (titanite, anorthite and baddeleyite) is able to accommodate significant amounts of thorium leads to a strong Th-enrichment in the residual glass of the partially crystallized layer which then induces ThO_2 crystallization (Fig. 3) because of the high Th^{4+} ion field strength F (F = 0.73, see below for F definition) [13]. In spite of thoria crystallization in the surface residual glass, it appears that ThO_2 concentration increases from 6.00 wt.% in the parent glass GTh (Table 1) to 7.70 wt.% in the surface residual glass at T_c = 1200 °C (Table 3). Moreover, EDX analysis shows that the thoria crystals formed at T_c = 1200 °C incorporated a low amount of zirconium ($Th_{0.95}Zr_{0.05}O_2$). This result is in agreement with the existence of a minor solid solution of ZrO_2 in ThO_2 as shown in the ZrO_2–ThO_2 phase diagram [81].

Table 2 also indicates that an important quantity of Zr^{4+} ions are substituted for Ti^{4+} ions in the titanite crystals for all the samples. This probably increases the chemical durability of titanite crystals due to the very low solubility of ZrO_2 in water (zirconate phases such as zircon, zirconolite and zirconia being well known for their very good chemical durability in water). Incorporation of zirconium in titanite crystals was also observed by Hayward in his GCM [58]. We may notice that the partial consumption of TiO_2 and ZrO_2 by titanite crystals could partly explain the absence of zirconolite crystals in the surface crystallized layer. The composition of surface residual glasses for the different samples given in Table 3 indicates that ZrO_2 content in the glassy phase was approximately divided by two in comparison with parent glasses which is accordance with the partial incorporation of Zr in titanite and in ThO_2 crystals. In their work on Zr partitioning between titanite and silicate melts, Prowatke et al. [60] also showed that zirconium was compatible with titanite (Zr partition coefficient > 1). Moreover, these authors also showed that contrary to Th and lanthanides, Zr partitioning did not significantly depend on Al_2O_3 content in parent glass.

In order to understand the evolution of the amount of Ln^{3+} ions incorporated in the titanite crystals formed near glass surface at T_c = 1200 °C according to the nature of the lanthanide (Table 2 and Fig. 4), we used the same approach as the one we already developed concerning the incorporation of actinide surrogates in the zirconolite crystals formed in the bulk of our GCM in [13]. The amount of lanthanides incorporated into titanite crystals was discussed in relation with the capacity of the glass to accommodate these elements (in accordance with their cationic field strength) and of the crystals to incorporate them in the calcium site of their structure (in accordance with bond valence-bond length considerations [70,71] developed to quantify the ability of the calcium site of the titanite structure to accept Ln^{3+} ions). In this paper we will only briefly recall the main points of the approach widely developed in [13]. Firstly, the tendency of lanthanide ions to separate from the glass (or more precisely from the supercooled melt during the heat treatment at $T_c > T_g$) can be correlated with their field strength F defined as $F = Z/d^2$ (in 1.6×10^{-19} C Å^{-2} unit) where Z is the cation charge and d is the cation–oxygen distance calculated as the sum of the cation and O^{2-} radii (with rO^{2-} = 1.4 Å [82]). Indeed, a general correlation exists between the tendency of a modifier cation (such as lanthanide ions in our glass compositions) to separate from glassy matrices and its field strength [83]: the higher its field strength the stronger its tendency to separate in other glassy or crystalline phases. Secondly, the ability of titanite crystals to incorporate lanthanide ions in the calcium site could be estimated by using both the site geometry (Ca^{2+}–O^{2-} distances in the structure) and a combination of the Pauling's electrostatic valence principle [84] and of the empirical bond valence (s) – bond length (R) model developed by Altermatt and Brown [70] and Brese and O'Keefe [71]. According to this model, the sum of the bond valences s_{Mj} between a given cation M – such as Ln^{3+} or Ca^{2+} in our case – and its j oxygen first neighbors must be equal to its valence (or oxidation state) V_M in a stable structure (in order to avoid important local structural distortions): $V_M = \sum_j s_{Mj}$. Consequently, the lower the difference $\Delta(M) = \left|V_M - \sum_j s_{Mj}\right|$, the higher the expected solubility of M in the structure. The valence of the individual M–O bonds s_{Mj} can be calculated from the bond lengths R_{Mj} (=distance between M and oxygen atom j) deduced from the titanite structure using the following relation: $s_{Mj} = \exp\left(\frac{R_0 - R_{Mj}}{B}\right)$ where R_0 is the bond valence parameter of M and B is a universal constant equal to 0.37 Å [85]. R_0 values for numerous cations are tabulated in literature [70,71] and varied as a function of the cation's valence but not as a function of the coordination number.

The bond valences were calculated for all the lanthanides (M = Ln) in the calcium site of titanite using the R_{Lnj} distances deduced from the weakly La-doped $Ca_{0.95}La_{0.05}Ti_{0.95}Al_{0.05}SiO_5$ structure determined by Hughes et al. [78]. The sums of the bond valences Σs_{Lnj} are given in Table 4 where they are compared with the lanthanides oxidation state V_{Ln}. It appears that in spite of its high field strength in the glass, Ce^{4+} ions could not be substituted for Ca^{2+} ions in titanite without strong distortions ($\Delta(Ce^{4+})$ = 1.68). As indicated above, tetravalent cerium ions are preferentially incorporated in the baddeleyite (ZrO_2) crystals. Divalent europium, that was detected by ESR in the parent glass GEu [13], is also una-

Table 4
Sum of the bond valences (Σs_{Lnj}) calculated for the different lanthanide (Ln) in the calcium site of titanite (coordination j = 7) using the crystallographic structural data of Hughes et al. [78] and the R_0 values taken from [71]. V_{Ln} is Ln oxidation state. Z/d^2 is the Ln cation field strength as defined in the text (in 1.6×10^{-19} C Å^{-2} unit). x corresponds to the amount of Ln ions incorporated by titanite formula unit (see Table 2).

	Ce^{3+}	Ce^{4+}	Nd^{3+}	Eu^{3+}	Eu^{2+}	Gd^{3+}	Yb^{3+}
R_0 (Å)	2.151	2.028	2.117	2.076	2.147	2.065	1985
Σs_{Lnj}	3.24	2.32	2.96	2.65	3.21	2.57	2,07
$V_{Ln} - \Sigma s_{Lnj}$	−0.24	1.68	0.04	0.35	−1.21	0.43	0,93
Z/d^2	0.46	0.78	0.48	0.52	0.29	0.52	0,58
x	0.07		0.11	0.10		0.12	0.06

dapted to be accommodated in the titanite calcium site ($\Delta(Eu^{2+}) = 1.21$) and probably remains in the surface residual glass as it is the case in the bulk [13]. Moreover, due to its low field strength ($F = 0.29$), the Eu^{2+} ion is certainly more soluble in the glass that all the other trivalent or tetravalent lanthanides (Table 4). For the trivalent lanthanides, the evolution of the Ln^{3+} ions field strength in the glass and of the difference $\Delta Ln^{3+} = \left|3 - (\sum_j s_{Lnj})\right|$ is reported in Fig. 7. This figure shows that, except for Yb^{3+} ions, $\Delta(Ln^{3+})$ remains relatively small for all the Ln^{3+} ions. These ions are thus relatively well suited to be incorporated into the titanite calcium site. Moreover, the fact that the field strengths of Nd^{3+}, Eu^{3+} and Gd^{3+} ions in the glass are relatively close (Table 4) could explain the low difference observed between the titanite composition for these three actinide surrogates (Table 2). The higher $\Delta(Yb^{3+})$ value indicates that the calcium site of titanite is not as well suited as for the other Ln^{3+} ions. This is probably at the origin of the smaller amount of ytterbium incorporated in the titanite crystals in spite of the high field strength of this ion in the glass (Table 4). The fact that a part of the cerium ions are incorporated into the baddeleyite (ZrO_2) crystals (probably as Ce^{4+} ions as indicated above) could explain the lower amount of cerium detected in titanite crystals (Table 2). It is also worth noting that whereas Gd and (Ce, Yb) exhibit respectively the highest and the lowest incorporation level x in the titanite crystals of the GCM (Fig. 4), Gd and (Ce, Yb) exhibit respectively the lowest and the highest concentrations in the surface residual glass (Fig. 6).

All these results concerning both Ln and Th distribution in the surface crystalline phases show that the lanthanides are mainly incorporated in the titanite crystals whereas thorium precipitates as thoria crystals. However, the amount of Ln and Th remains high in the surface residual glass (Table 3, Fig. 6). Consequently, it could be assumed that trivalent minor actinides such as Am^{3+} and Cm^{3+} ions (for which Nd^{3+}, Gd^{3+} and Eu^{3+} ions can be considered as good simulants) would be also immobilized in the titanite crystals and in the residual glass of the surface crystallized layer. Concerning the tetravalent actinides such as Np^{4+} and Pu^{4+}, the results obtained in this work for the thorium-doped sample might lead to more pessimistic conclusions and these actinide ions could partly precipitate as actinide dioxide in the partially crystallized layer. However, it must be underlined that strong differences were reported in literature concerning for instance the solubility behavior of Pu^{4+} and Th^{4+} ions in ZrO_2 [77]. Thus, we cannot definitively conclude concerning the behavior of Np^{4+} and Pu^{4+} ions in the surface layer of our GCM. Nevertheless, we must keep in mind that the thickness of the crystallized layer remains relatively limited (<1 mm) if we use the nucleation (2 h) + crystal growth (2 h) glass–ceramic synthesis method (Fig. 2). Moreover, in previous works [43] we showed that the best results concerning the incorporation of actinide surrogates in the zirconolite crystals formed in the bulk were obtained for $T_c = 1050$ °C. At this temperature the thickness of the crystallized layer do not exceed 200 μm (Fig. 2). The good resistance of crystallized or metamict titanite samples to chemical alteration – essentially due to the high TiO_2 concentration – reported by Hayward [58] indicates that the formation of this phase (that incorporates a fraction of actinide surrogates in our study) on the surface of the zirconolite-based GCM would be probably not deleterious to their long term behavior. It must be underlined that, as indicated above, the fact that a part of the Ti^{4+} ions in the titanite structure is replaced by Zr^{4+} ions in our samples (Table 2) will probably increase their chemical durability. Moreover, the composition of the silica-rich residual glass remaining between the crystallized phases of the surface for the GCM prepared at $T_c = 1200$ °C (Table 3) indicates that this glass has probably a higher chemical durability than the classical borosilicate nuclear glasses currently used to incorporated HLW. Indeed, the absence of B_2O_3, the low Na_2O concentration and the occurrence of significant amounts of both CaO, Al_2O_3, ZrO_2, TiO_2 and Ln_2O_3 are known to increase the glass durability in water [55,86–89]. All these results show that, at least for the trivalent actinides, the formation of a thin partially crystallized layer from the surface of our GCM (using a 2 h crystal growth heat treatment) would not be so much deleterious to their chemical durability. However, during the alteration by water of the surface of GCM, Ln and Th releases will be mainly controlled by the residual glassy phase which is less durable than the crystalline phases able to incorporate these elements in the surface layer.

4.3. Effect of the concentration of trivalent actinide surrogate (Nd) on the nature, the structure and the composition of the crystals growing from glass–ceramic surface

This study was only performed for the Nd-doped samples prepared at $T_c = 1050$ °C and 1200 °C with Nd_2O_3 concentration in the parent glass ranging from 0 to 10 wt.% (Table 1). The effect of the Nd_2O_3 concentration on zirconolite crystallization in the bulk of the glass (nucleation rate, structure and composition of zircon-

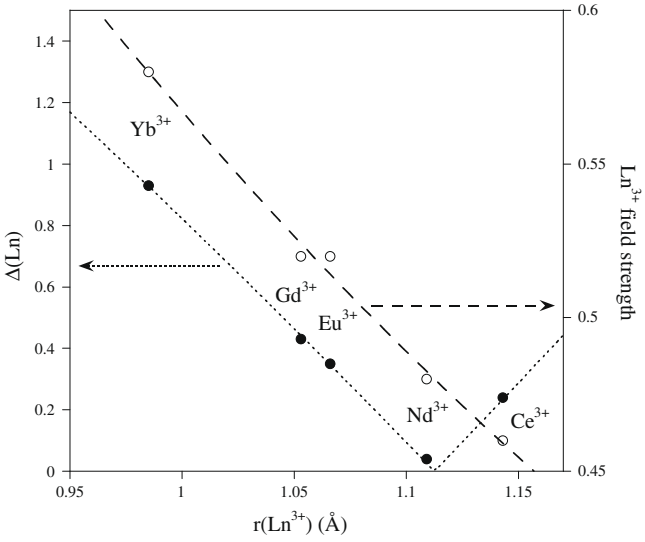

Fig. 7. Evolution of the Ln^{3+} ions field strength in the glass (Table 4) and of the difference $\Delta Ln = \left|V_{Ln} - (\sum_j s_{Lnj})\right|$ in the calcium site of titanite (Table 4) as a function of the lanthanide size (in 8-fold coordination [82]).

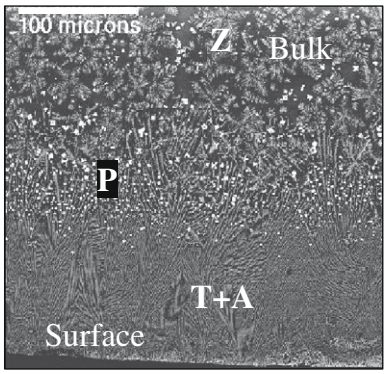

Fig. 8. Back-scattered SEM image of the 10 wt.% Nd-doped GCM heat treated at $T_c = 1050$ °C showing the interface (containing perovskite crystals) between the bulk (containing zirconolite crystals) and the surface crystallized layer (containing titanite + anorthite crystals). A: anorthite, P: perovskite, T: titanite, Z: zirconolite.

Table 5
Compositions determined by EDX for the titanite, baddeleyite and anorthite crystals formed in the surface crystallized layer at T_c = 1200 °C as a function of the Nd_2O_3 concentration (wt.%) in the parent glass. Titanium was assumed to occur only as Ti^{4+} in all crystals. /: composition not determined, □: calcium vacancy.

Nd_2O_3 wt.%	Titanite	Anorthite	Baddeleyite
0	$Ca_{0.99}Ti_{0.78}Zr_{0.23}Al_{0.02}Si_{0.98}O_5$	$Ca_{0.78}Na_{0.17}\square_{0.05}Al_{1.73}Si_{2.27}O_8$	/
1	$Ca_{0.97}Nd_{0.025}Ti_{0.77}Zr_{0.215}Al_{0.04}Si_{0.98}O_5$	/	/
2	$Ca_{0.95}Nd_{0.045}Ti_{0.765}Zr_{0.22}Al_{0.06}Si_{0.97}O_5$	/	/
6	$Ca_{0.89}Nd_{0.11}Ti_{0.69}Zr_{0.22}Al_{0.11}Si_{0.98}O_5$	$Ca_{0.77}Na_{0.19}\square_{0.04}Al_{1.73}Si_{2.27}O_8$	$Zr_{0.93}Ti_{0.07}O_2$
10	$Ca_{0.84}Nd_{0.16}Ti_{0.67}Zr_{0.21}Al_{0.16}Si_{0.96}O_5$	$Ca_{0.77}Na_{0.18}\square_{0.05}Al_{1.72}Si_{2.28}O_8$	$Zr_{0.93}Ti_{0.07}O_2$

olite crystals) was reported in [72]. At the two temperatures and for all the Nd-doped GCM, the formation of a partially crystallized layer is observed. At T_c = 1200 °C, the thickness of this layer always remains lower than 1 mm and it is constituted of titanite + anorthite + baddeleyite crystals + residual glass. However, for the highly Nd-doped samples (8 and 10 wt.% Nd_2O_3) heat treated at T_c = 1050 °C, the formation of a new crystalline phase (perovskite) is observed at the interface between the bulk (containing residual glass + zirconolite crystals) and the crystallized layer (Fig. 8). The composition of these perovskite crystals was already presented in [72] and it appeared that they were able to incorporate high neodymium amounts, mainly in the calcium site of their structure following the formula $CaNd_{0.34}\square_{0.17}TiO_3$ (□: calcium ion vacancy) for the GNd10 sample. It can be notice that Hayward [58] also reported the formation of Ln-rich perovskite crystals in the bulk of several of his titanite-based GCM.

The composition of the crystalline phases formed at T_c = 1200 °C in the layer is given in Table 5 for several samples with increasing Nd_2O_3 concentrations and the composition of the residual glass is reported in Table 3. The composition of the anorthite and baddeleyite (ZrO_2) crystals is not affected by the simulant concentration. As for the Ln-doped samples studied above, it appears that titanite always remains the only crystalline phase of the layer able to incorporate the Nd^{3+} ions. As previously, the Nd^{3+} ions are substituted in the calcium site of the titanite structure with charge compensation ensured by Al^{3+} ions. Fig. 9 shows that the amount of neodymium incorporated in titanite increases continuously with the Nd_2O_3 concentration in the parent glass. This is in agreement with the nearly linear evolution of the lattice parameters of titanite crystals determined by XRD (Fig. 10). These results show that no saturation effect occurs concerning Nd incorporation in the titanite crystals of the layer at least for Nd_2O_3 concentrations less than or equal to 10 wt.% in the parent glass. However, even for the GNd10 sample, the amount of Nd^{3+} ions incorporated in the Ca^{2+} site (16 mol%, Fig. 9) remains lower than the solubility limit of La_2O_3 in titanite reported in literature for the $Ca_{1-x}La_xTi_{1-x}Al_xSiO_5$ ceramic (20 mol%) [80].

The comparison of the composition of the residual glass remaining between the crystals of the surface layer (T_c = 1200 °C, Table 3) with that of the corresponding composition of Nd-bearing parent glasses (Table 1) confirms the results already given and discussed above in Section 4.2 for the GNd6 sample. Furthermore, neodymium concentration in the residual glass of surface increases almost linearly with total neodymium concentration (Fig. 5). For all neodymium contents, the amount of Nd_2O_3 always remains slightly higher in residual glass than in parent glass (Fig. 5). It also appears that Nd_2O_3 concentration is slightly higher in the residual glass near the surface than in the bulk and the difference increases with total neodymium concentration.

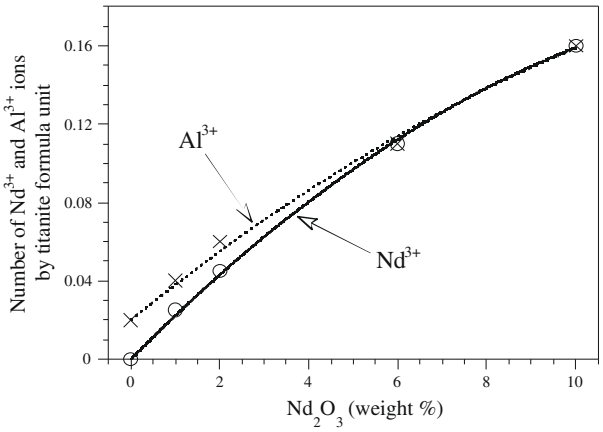

Fig. 9. Evolution of the number of Nd^{3+} and Al^{3+} ions by formula unit (see Table 5) in the titanite crystals formed in the crystallized layer near the surface of the Nd-doped GCM prepared at T_c = 1200 °C as a function of the Nd_2O_3 concentration in the parent glass.

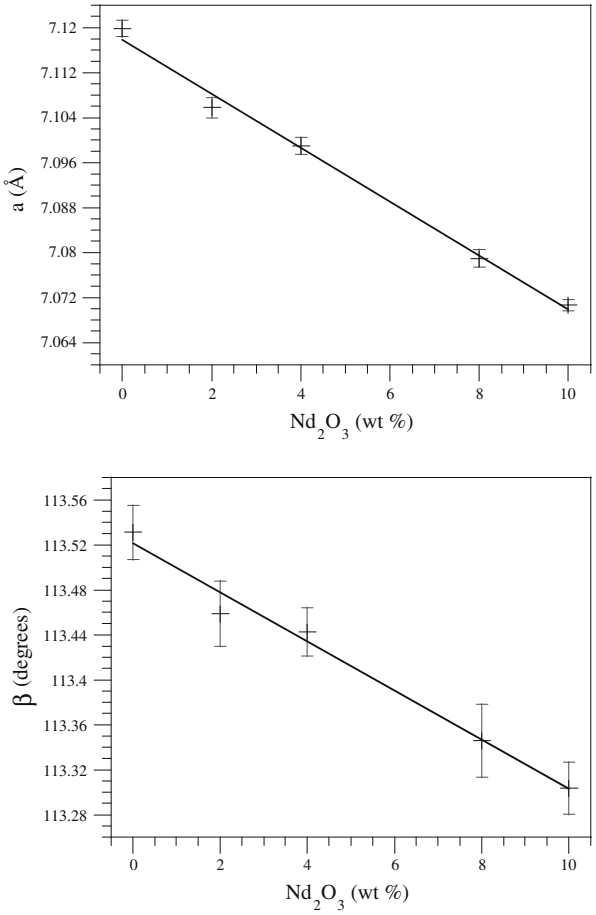

Fig. 10. Evolution of the a and β lattice parameters of titanite (monoclinic structure) crystals formed in the crystallized layer near the surface of the Nd-doped GCM prepared at 1200 °C (2 h) as a function of the Nd_2O_3 concentration in the parent glass.

4.4. Competition between the growth of the surface crystallized layer and the zirconolite crystals in the bulk for long duration heat treatments

The evolution at 1050 °C and 1200 °C of the nature of the crystalline phases formed in the bulk and near the surface of the GCM for increasing thermal treatment durations between 2 h and 300 h was studied for the Nd-, Eu-, Gd-, Th-doped and undoped GCM (Table 6). In Fig. 11 are presented several SEM images showing the evolution of the bulk of the GCM after heat treatment during different durations at 1050 °C or 1200 °C. Moreover, the XRD patterns of the bulk of the GNd6 GCM prepared at T_c = 1050 °C for durations ranging from 2 h to 300 h were also recorded and the crystalline phases were identified (Fig. 12). It is important to recall that the size of our samples do not exceed 1 cm diameter which implies that for long duration heat treatments, the crystals growing from the surface can reach the bulk of the sample. The study of these different results clearly shows that:

– At 1200 °C (temperature for which the growth kinetics of the surface layer is near its maximum, Fig. 2) for the 20 h heat treatment, the titanite and anorthite crystals initially present in the thin crystallized layer near sample surface after the 2 h thermal treatment (Fig. 3b), grow towards the bulk at the expense of the

Table 6
Crystalline phases formed in the bulk and near the surface of the Nd-, Eu-, Gd-, Th-doped (respectively GNd6, GEu, GGd and GTh) and the undoped (G0) GCM for different durations of crystal growth heat treatment at T_c = 1050 °C and 1200 °C.

Crystal growth thermal treatment	Surface	Bulk
G0, GNd6, GEu, GGd samples		
2 h 1050 °C	Titanite + Anorthite	Zirconolite
20 h 1050 °C	Titanite + Anorthite + Wollastonite	Zirconolite + Anorthite + Wollastonite + Apatite[b]
300 h 1050 °C[a]	Titanite + Anorthite + Wollastonite + Cristobalite	Zirconolite + Anorthite + Wollastonite + Titanite + Cristobalite + Apatite[b]
2 h 1200 °C	Titanite + Anorthite + Baddeleyite	Zirconolite
20 h 1200 °C	Titanite + Anorthite + Baddeleyite	Titanite + Anorthite + Baddeleyite
GTh sample		
2 h 1050 °C	Titanite + Anorthite + Thoria	Zirconolite
20 h 1050 °C	Titanite + Anorthite + Wollastonite + Thoria	Zirconolite + Thoria
2 h 1200 °C	Titanite + Anorthite + Thoria + Baddeleyite	Zirconolite
20 h 1200 °C	Titanite + Anorthite + Thoria + Baddeleyite	Titanite + Anorthite + Thoria + Baddeleyite

[a] The thermal treatment for 300 h at 1050 °C was only performed for the GN6 sample.
[b] Apatite was not observed for the G0 sample.

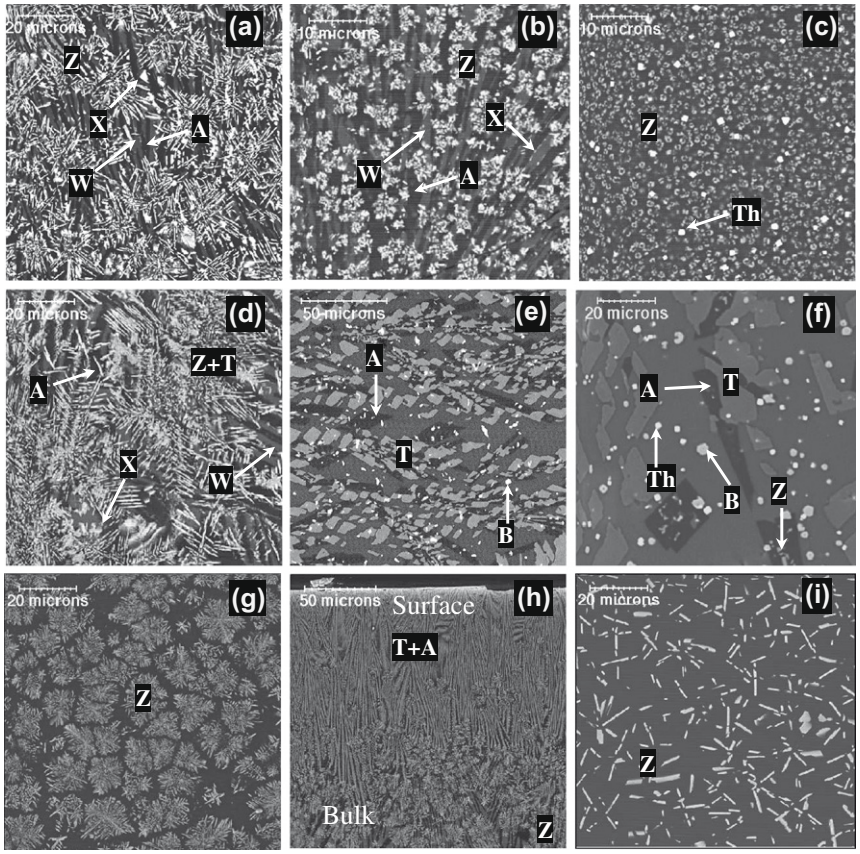

Fig. 11. Back-scattered SEM images of the bulk of the GCM heat treated: for 20 h at T_c = 1050 °C: samples GNd6 (a), GGd (b), GTh (c); – for 300 h at T_c = 1050 °C: sample GNd6 (d); for 20 h at T_c = 1200 °C: samples G0 (e), GTh (f); for 2 h at T_c = 1050 °C (g, h) and T_c = 1200 °C (i): sample GNd6.

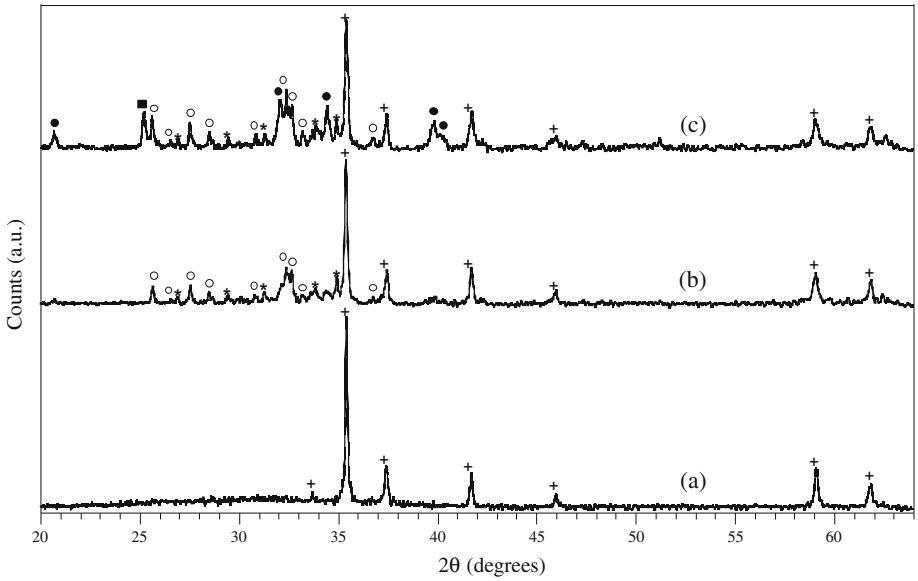

Fig. 12. XRD patterns (λCoK_α) of the bulk of GNd6 GCM for different durations of crystal growth heat treatment at T_c = 1050 °C: (a) 2 h, (b) 20 h, (c) 300 h. +: zirconolite, ○: anorthite, ●: titanite, ■: cristobalite, *: wollastonite.

zirconolite crystals previously formed (Fig. 11e). This evolution is observed for all the Ln-doped, Th-doped and undoped samples (Table 6). For all these GCM, baddeleyite (ZrO_2) crystals are also observed in the bulk, coexisting with titanite and anorthite. However, for the Th-doped sample, thoria crystals are also detected in the bulk (Fig. 11f). This indicates that the zirconolite crystals formed initially in the bulk after a 2 h crystal growth heat treatment (Fig. 11i), are unstable with respect to titanite and anorthite in the presence of the residual glass. Thus, at high temperature (1200 °C) and for a long duration heat treatment, the growth of titanite crystals from the surface progressively consumes the zirconolite crystals of the bulk, and the excess of ZrO_2 (that is only partially incorporated in the titanite crystals as shown in Table 2) precipitates as baddeleyite crystals in the residual supercooled melt (Table 6). The fact that zirconolite and titanite crystals do not coexist in the bulk in our system could be explained by the fact that the amount of TiO_2 in parent glasses is probably not high enough for the coexistence of these two titanate phases. For instance, for the GNd6 sample, the amount of TiO_2 in parent glass strongly decreases from 11.14 mol% to 4.30 mol% in the residual glass of the crystallized layer (see Section 4.2, Tables 1 and 3).

– At 1050 °C, the progression of titanite crystals towards the bulk becomes very slow in comparison with anorthite and the growth kinetics of the surface layer strongly decreases (Fig. 2). This can be due both to the increase of the supercooled liquid viscosity and to the decrease of the dissolution rate of zirconolite at 1050 °C. After 20 h heating, the zirconolite crystals initially formed in the bulk (Fig. 11g, h after 2 h heating) are still observed (Table 6 and Fig. 11a–c), their microstructure is not affected (compare for instance Fig. 11a, g) and titanite crystals remain located near samples surface (Table 6). However, the growth in the bulk of anorthite crystals from the surface for the Nd-, Gd- and Eu-doped and undoped samples is observed (Table 6, Figs. 12 and 11a, b). In these conditions, baddeleyite crystals are not detected in the bulk which seems to confirm the fact that the formation of ZrO_2 is associated with the disappearance of zirconolite. Moreover, XRD (Fig. 12) and EDX results indicate the formation of a new crystallized silicate phase, wollastonite (nominally $CaSiO_3$), both in the surface layer and in the bulk after 20 h heating. It is interesting to notice that wollastonite is not observed near the surface of the GCM heated at 1050 °C for 2 h or at 1200 °C for 2 h or 20 h. This indicates that this phase probably crystallizes from the surface residual glass and is not stable at T = 1200 °C in our system. Crystallization of wollastonite is not surprising because of the high SiO_2 and CaO contents remaining in the residual glass. For the Th-doped sample, the anorthite and wollastonite crystals only remain in the crystallized layer and are not observed in the bulk (Table 6 and Fig. 11c). These differences between the Th-doped sample and the other ones could be explained by the very high zirconolite nucleation rate for the glass containing thorium ions because of their high field strength [13]. In these conditions, the numerous zirconolite crystals formed in the bulk probably disturb the crystal growth of both anorthite and wollastonite towards the bulk. The high field strength of thorium ions could also explain the precipitation of ThO_2 in the bulk of Th-doped sample (Table 6 and Fig. 11c). For the GNd6 GCM prepared at 1050 °C for 20 h, several zones containing a Nd-rich phase are observed on the SEM images (Fig. 11a). Similar Ln-rich zones are not clearly detected for the other samples. EDX analysis of these zones shows that they essentially contain SiO_2, CaO and Nd_2O_3 in the following molar proportions: 4/2/1. As no crystalline phase containing these oxides with this molar ratio is reported in our XRD data base [90], we prepared and heated a $8SiO_2$–4CaO–$1Nd_2O_3$ mixture (see the experimental part in Section 3). The corresponding XRD pattern given in Fig. 13 clearly shows that the Nd-rich phase is in fact a cristobalite + Nd-apatite mixture. Comparison with other studies of the authors [14,91] on the crystallization of lanthanide-rich aluminoborosilicate glasses developed to immobilize highly concentrated waste solutions arising from the reprocessing of high burn-up nuclear spent fuel indicate that this apatite-type phase is probably $Ca_2Nd_8(SiO_4)_6O_2$. This phase was also reported by Hayward [58] in titanite-based GCM for several samples. It is interesting to notice that lanthanide silicate apatite phases were firstly proposed as host phase for the lanthanides in the supercalcine multiphase ceramics developed for the immobilization of highly radioactive wastes more than thirty years ago [92,93]. The impact of α-decay on the structure and chemical durability against water of actinide-doped Nd silicate apatite ceramics was also reported in literature [94].

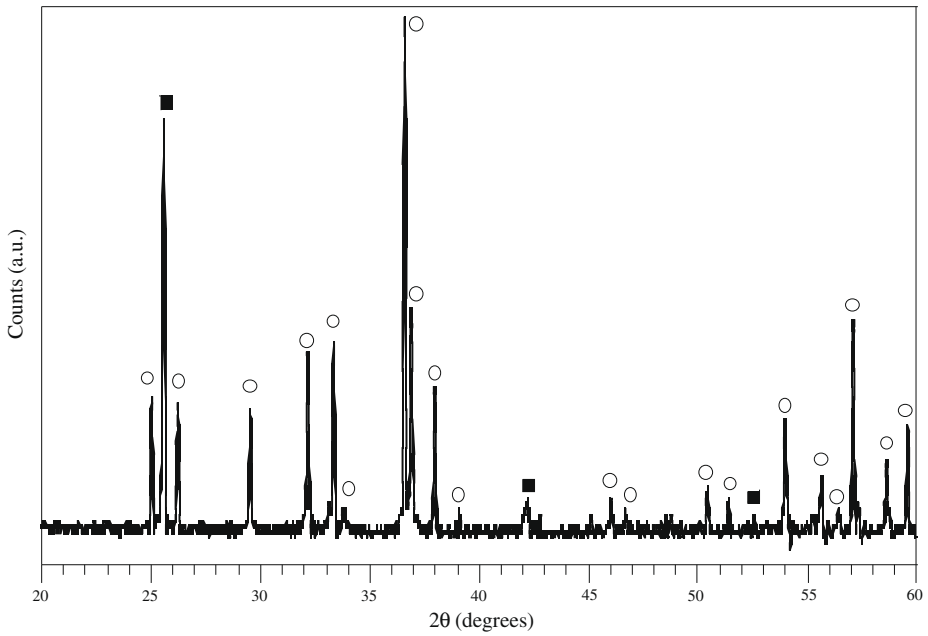

Fig. 13. XRD pattern (λCoK_α) of a ceramic sample prepared from a $8SiO_2$–$4CaO$–$1Nd_2O_3$ (molar proportions) mixture during 25 h at 1400 °C and 25 h at 1500 °C. ■: cristobalite, ○: apatite.

– Even after 300 h at 1050 °C (only the GNd6 sample was studied in these conditions), a high amount of zirconolite remains in the bulk (Table 6 and Fig. 11d). However, in this case, a small proportion of titanite crystals has also grown in the bulk at the expense of zirconolite (Figs. 8d and 12c). Cristobalite crystals are also detected in the bulk in these conditions.

In order to follow the incorporation of Nd^{3+} ions in the different crystalline phases formed at 1050 °C in the surface layer and in the bulk both for short (2 h) and long (300 h) heat treatment durations, we recorded the optical absorption (Fig. 14) and ESR (Fig. 15) spectra of: the parent glass GNd6, the surface crystallized layer (2 h) and the bulk of the GCM (2 h and 300 h). Spectra were also

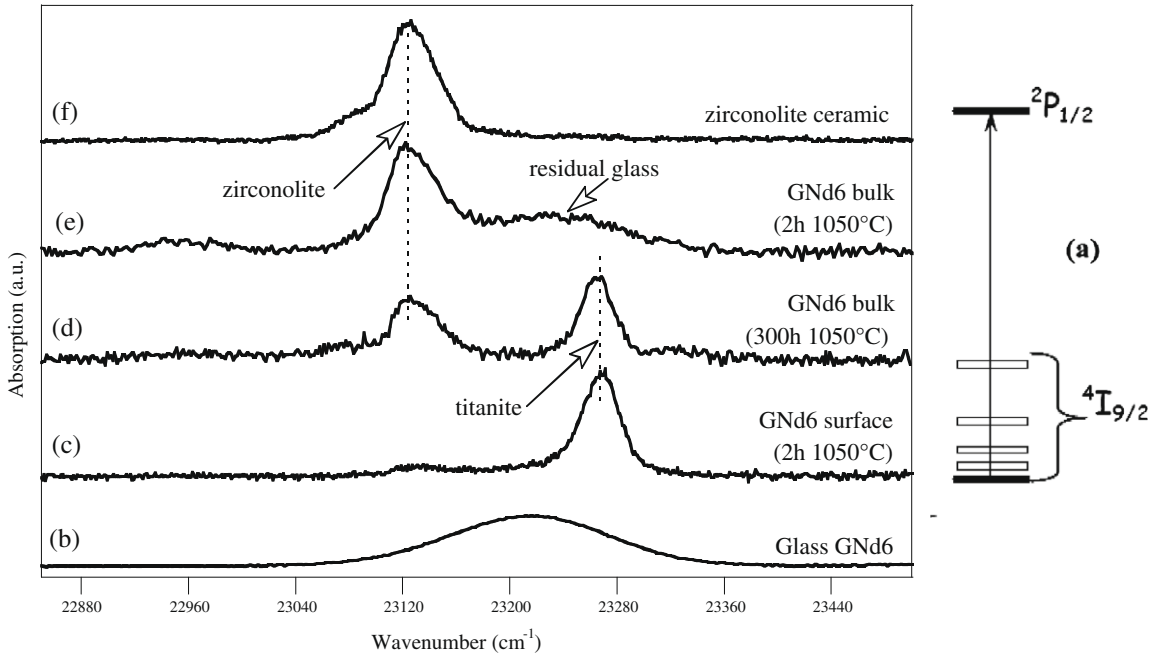

Fig. 14. Neodymium optical absorption spectra corresponding to the $^4I_{9/2} \rightarrow {}^2P_{1/2}$ transition. (a) Scheme showing the transition from the lowest Stark level of the $^4I_{9/2}$ state to the non-degenerated $^2P_{1/2}$ excited state. The $^4I_{9/2}$ ground state of neodymium ion is splitted into five Stark (or Kramers) doublets under the action of a low symmetry crystal field. This is the case for Nd^{3+} ions in the calcium site of C_1 symmetry in zirconolite. At $T \approx 10$ K only the lowest Stark doublet of the $^4I_{9/2}$ state is populated. As the degeneracy of the $^2P_{1/2}$ state is not removed by the crystal field occurring around Nd^{3+} cations, each kind of neodymium environment is characterized by only one $^4I_{9/2} \rightarrow {}^2P_{1/2}$ absorption band at low temperature. Spectra recorded at low temperature ($T < 15$ K) for: (b) the parent glass GNd6, (c) the surface crystallized layer of the GNd6 GCM heat treated at $T_c = 1050$ °C for 2 h, (d) the bulk of the GNd6 GCM heat treated for 300 h at $T_c = 1050$ °C, (e) the bulk of the GNd6 GCM heat treated for 2 h at $T_c = 1050$ °C, (f) the $Ca_{0.7}Nd_{0.3}ZrTi_{1.7}Al_{0.3}O_7$ zirconolite ceramic. The optical absorption bands associated with Nd^{3+} ions in titanite and in zirconolite are indicated in the figure. The slight contribution near 22,950 cm^{-1} on the spectrum of the bulk of the GCM (2 h 1050 °C) can be attributed to the incorporation of a low amount of Nd^{3+} ions in the zirconium site of zirconolite [9].

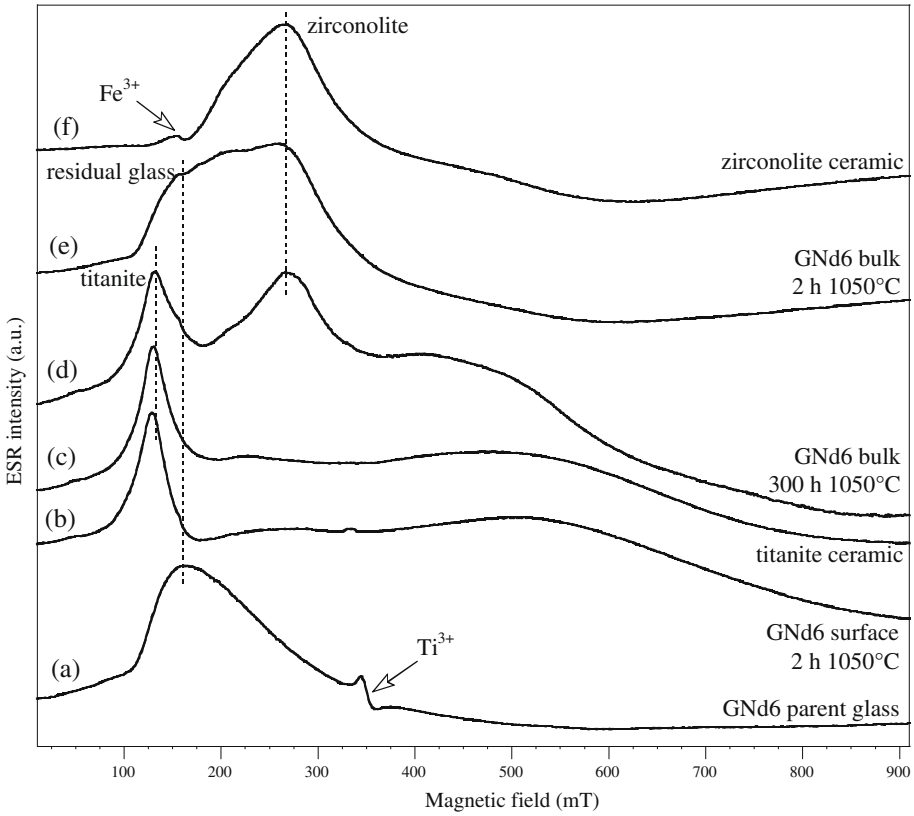

Fig. 15. Neodymium ESR spectra recorded at $T = 12$ K for the: (a) parent glass GNd6, (b) surface crystallized layer of the GNd6 GCM heat treated at $T_c = 1050$ °C for 2 h, (c) $Ca_{0.88}Nd_{0.12}Ti_{0.70}Zr_{0.18}Al_{0.12}Si_{1.00}O_5$ titanite ceramic, (d) bulk of the GNd6 GCM heat treated for 300 h at $T_c = 1050$ °C, (e) bulk of the GNd6 GCM heat treated for 2 h at $T_c = 1050$ °C, (f) $Ca_{0.7}Nd_{0.3}ZrTi_{1.7}Al_{0.3}O_7$ zirconolite ceramic. The small contributions due to both Fe^{3+} ($3d^5$) paramagnetic impurities and Ti^{3+} ($3d^1$) ions originating from a slight reduction of Ti^{4+} ions in the parent glass during melting are indicated in the figure.

recorded for two Nd-doped ceramics serving as reference samples: $Ca_{0.7}Nd_{0.3}ZrTi_{1.7}Al_{0.3}O_7$ zirconolite and $Ca_{0.88}Nd_{0.12}Ti_{0.70}Zr_{0.18}Al_{0.12}Si_{1.00}O_5$ titanite. The compositions of these phases are close to those of the zirconolite and titanite crystals formed in the Nd-doped GCM (see Table 2 and [13,72]). The study of Figs. 14 and 15 confirms the results obtained by SEM, EDX and XRD given above concerning both the incorporation of Nd^{3+} ions in zirconolite and titanite phases and the formation of titanite in the bulk for long duration heat treatments. It clearly appears that both the $^4I_{9/2} \rightarrow {}^2P_{1/2}$ optical transition band and the ESR signal strongly depend on the matrix in which neodymium ions are incorporated. For instance, because of the lack of long-range order in glasses, the environment around neodymium ions slightly differs from site to site in the glassy network, the $^4I_{9/2} \rightarrow {}^2P_{1/2}$ optical transition band of Nd^{3+} ions in the parent glass (Fig. 14b) and in the residual glass (Fig. 14e) are inhomogeneously broadened. In comparison, the optical absorption of Nd^{3+} ions in zirconolite ceramic appears as relatively thin bands on the spectrum (Fig. 14f). As titanite is the only crystalline phase in the surface crystallized layer that incorporates Nd^{3+} ions in its structure (Tables 2 and 5), the thin absorption band observed near 23,280 cm^{-1} in Fig. 14c can be attributed to Nd^{3+} ions located in the Ca site of titanite crystals. This is confirmed if we compare the ESR spectra of neodymium in $Ca_{0.88}Nd_{0.12}Ti_{0.70}Zr_{0.18}Al_{0.12}Si_{1.00}O_5$ titanite ceramic (Fig. 15c) and in the crystallized layer (Fig. 15b). The comparison of the optical and ESR spectra of the parent glass and ceramics on one hand with those of the crystallized layer and of the bulk of the GCM on the other hand shows that:

- In the crystallized layer, Nd^{3+} ions are mainly incorporated in the titanite phase (Figs. 14c and 15b, c). Signals associated with neodymium in other crystalline phase are not detected which in accordance with EDX results (Tables 2 and 5). Moreover, because of the relatively high crystallinity of this layer (Fig. 3) in comparison with that of the bulk of the GCM heat treated during 2 h (Fig. 11g, i), the contribution of neodymium in the surface residual glass is difficult to detect by optical absorption or ESR.
- In the bulk of the GCM (2 h thermal treatment, Figs. 14e and 15e), Nd^{3+} ions are located both in the zirconolite crystals and in the residual glass.
- In the bulk of the GCM (300 h thermal treatment), Nd^{3+} ions are located both in zirconolite and titanite crystals. The occurrence of two optical absorption bands associated with these two phases is clearly detected on the spectrum (Fig. 14d). The simultaneous contribution of these two phases is also evident on the ESR spectra (Fig. 15d). Moreover, the contribution of residual glass to the spectra becomes difficult to detect which can be explained both by an increase of crystallinity in the bulk and by the incorporation of a fraction of neodymium ions in titanite.

All these results concerning the effect of the crystal growth thermal treatment duration on glass crystallization and more specifically on the competition between bulk and surface crystallization, shows that zirconolite – initially formed in the bulk of all the doped and undoped samples after 2 h thermal treatment – is a metastable phase in the system studied here which contains both titanite and a silica-rich residual glass. Thus, titanite can be considered as the most stable phase incorporating Ti in this system. However, by heating a titanite + zirconolite ceramics mixture at 1200–1280 °C for 2 days, Vance et al. [80] showed that zirconolite and titanite could coexist thermodynamically. It is very important to

notice that in their study, there was not silica excess in their mixture (Si is one of the main element in titanite composition) as it is the case in our work (occurrence of a silica-rich residual glass). Hayward [58] also reported for several of the titanite-based GCM he studied (and more particularly for the Ln_2O_3-rich ones), the crystallization at relatively low temperature (850–900 °C) of intermediate phases such as the pyrochlore-structure $(Ca, Ln)_2Ti_2O_7$ in the bulk of the glass. These metastable phases then react with excess silica to form titanite. This is probably the same kind of phenomena that occurs in our samples (but at higher temperature) when the titanite crystals grow towards the bulk of the samples giving schematically the following reaction:

$$CaTiSiO_{5(\text{growing towards the bulk})} + CaZrTi_2O_{7(\text{bulk})} + SiO_{2(\text{bulk residual glass})} \Rightarrow CaTiSiO_5 + ZrO_2$$

For kinetics reasons due to its relatively high nucleation rate in the bulk, zirconolite is the only crystalline phase that nucleates and grows in the bulk for relatively short crystal growth heat treatments (2 h) at T_c = 1050 °C or 1200 °C (Fig. 11g, i). However, titanite which nucleates only on sample surface can lead – under particular conditions during the GCM preparation – to the disappearance of the zirconolite crystals formed initially in the bulk at least on the centimetric size samples of this study. This is the case if both the crystal growth temperature T_c is relatively high (1200 °C) and if the heating duration is relatively long (20 h). The occurrence or not of actinide surrogates and their nature has no effect on these phenomena. Consequently, as nucleation of titanite on glass surface cannot be avoided, in order to reduce the risks of progression of the titanite crystals from the surface towards the bulk of the GCM at the expense of zirconolite (Fig. 11h), T_c must not be too high and/or the heating duration at this temperature must not exceed a few hours. In these conditions, titanite crystals will remain located in a thin crystallized layer (Fig. 2) that will probably not affect the long term behavior of the waste form as indicated above due to the good chemical durability of this phase. Moreover, an increase of the zirconolite nucleation rate in the bulk could lead to a decrease of the thickness of the crystallized layer.

Even if zirconolite is a metastable phase in the system studied here, the evolution of the bulk of the waste form will not happen during storage or disposal because surface and internal temperatures of the waste form (for minor actinides amounts $\leqslant$ 10 wt.%) will never reach values lying in the nucleation and crystal growth ranges. Indeed, during storage and disposal, the temperature in the bulk of the waste form will remain lower than the glass transformation temperature T_g ($T < T_g \approx 760$ °C for the residual glass in the bulk [95]) and a very high kinetic barrier will control the long-range diffusion processes associated with titanite crystal growth in the glassy state. During the first centuries after waste form fabrication, the main contribution to the thermal power will be due to Cm disintegration and more particularly to ^{244}Cm isotope (half live $\approx$ 18 years). However, this radionuclide only represents about 3 wt.% of all minor actinides [96]. Consequently, zirconolite will remain kinetically stable and no long-term evolution of both the structure and microstructure of the GCM are expected to occur in these conditions.

5. Conclusions

In a previous paper [13], we reported the effect of the nature of minor actinide or Pu surrogates on internal crystallization in SiO_2–Al_2O_3–CaO–ZrO_2–TiO_2 glasses that led to potential glass–ceramic host materials for the immobilization of these long-lived radionuclides. In this case, it appeared that for all the simulants (Ce, Nd, Eu, Gd, Yb, Th) introduced in the parent glass composition, the highly durable zirconolite crystals were the only ones to nucleate in the bulk of the glass. However, the formation of a thin partially crystallized layer containing mainly titanite and anorthite crystals was also observed but was not studied. In order to complete this previous work, the aim of the present paper was to study the effect of the nature of surrogates on the structure, the microstructure and the composition of the crystals formed in the layer near the surface of the GCM and of the residual glass remaining between these crystals. The study of the competition between surface crystallization and internal crystallization was also one of the aims of this work. The main conclusions that can be drawn from this study are the following:

i. For all the samples, titanite and anorthite are the main crystalline phases present in the surface layer for T_c = 1050 °C and 1200 °C. For T_c = 1200 °C, small baddeleyite (ZrO_2) crystals are also observed independently of the nature of the actinide surrogate. However, for the Th-doped GCM, ThO_2-rich crystals also precipitate in the layer for the two crystal growth temperatures. In all cases, the thickness of the layer was shown to increase with T_c from 170 to 190 μm (1050 °C) to 500 to 1000 μm (1200 °C). Titanite is the only crystalline phase in the layer able to incorporate significant quantities of Ln^{3+} trivalent lanthanide ions in the Ca site of its structure. In this case, the positive charge excess due to Ln^{3+} ions incorporation is compensated by the simultaneous incorporation of Al^{3+} ions probably both in the titanium and silicon sites of titanite. Comparison with our previous results [13] shows that the zirconolite crystals of the bulk are more efficient to incorporate actinide surrogates than the titanite crystals formed near samples surface. However, the amount of titanite in the layer is greater than that of zirconolite in the bulk. Nevertheless, a high proportion of surrogate remains in the residual glass of the layer. An evolution of the amount of Ln^{3+} ions incorporated in the titanite crystals formed at T_c = 1200 °C according to the nature of the lanthanide is observed. This evolution is explained by considering both the capacity of the glass to accommodate these elements (in accordance with their cationic field strength) and the capacity of the titanite crystals to incorporate them in the calcium site of their structure (in accordance with bond valence-bond length considerations). No significant amount of Th^{4+} ions is incorporated in titanite crystals at T_c = 1200 °C which could be explained by the very low solubility limit of ThO_2 in titanite following the incorporation scheme $Ca_{1-x}Th_xTi_{1-2x}Al_{2x}SiO_5$ in accordance with literature. The fact that none of the crystalline phases (titanite, anorthite and baddeleyite) of the surface layer is able to accommodate significant amounts of thorium leads to a strong Th-enrichment in residual glass of the layer which explains ThO_2 precipitation. Consequently, it can be assumed that trivalent minor actinides such as Am^{3+} and Cm^{3+} ions (for which Nd^{3+}, Gd^{3+} and Eu^{3+} ions are considered as good simulants) will be immobilized in the titanite crystals and in the residual glass of the surface layer. Concerning the tetravalent actinides such as Np^{4+} and Pu^{4+}, the results obtained in this work for the thorium-doped sample lead to more pessimistic conclusions because these actinide ions could partly precipitate as actinide dioxide in the surface layer.

ii. The effect of Nd_2O_3 concentration (from 0 to 10 wt.%) in parent glass on the formation of the partially crystallized layer was studied. For all the Nd-doped samples, the layer is constituted of titanite, anorthite and baddeleyite (at T_c = 1200 °C) crystals and of a residual glass. Titanite remains the only crystalline phase of the layer able to incorporate the Nd^{3+} ions with charge compensation ensured by Al^{3+} ions and the amount of neodymium incorporated increases con-

tinuously with the Nd_2O_3 concentration in the parent glass. These results show that no saturation effect occurs concerning Nd incorporation in the titanite crystals at least for Nd_2O_3 concentrations less than or equal to 10 wt.% in the parent glass.

iii. The evolution at 1050 °C and 1200 °C of the nature of the crystalline phases formed in the bulk and near the surface of the GCM was studied for increasing thermal treatment durations for the Nd-, Eu-, Gd-, Th-doped and the undoped GCM (cylindrical samples of 1 cm diameter). At 1200 °C (for the 20 h heat treatment), the titanite and anorthite crystals grow towards the bulk at the expense of the zirconolite crystals previously formed. Baddeleyite (ZrO_2) crystals are also observed in the bulk, coexisting with titanite and anorthite. For the Th-doped sample, ThO_2-rich crystals are also detected in the bulk. Thus, the zirconolite crystals formed initially in the bulk after the 2 h crystal growth heat treatment, are unstable with respect to titanite in the presence of the silica excess of the residual glass: at 1200 °C, the growth of titanite from the surface progressively consumes the zirconolite crystals of the bulk, and the excess of ZrO_2 (only partially incorporated in the titanite crystals) precipitates as baddeleyite crystals. At 1050 °C, the progression of titanite crystals towards the bulk becomes very slow in comparison with anorthite and the growth kinetics of the surface layer strongly decreases. After 20 h heating, the zirconolite crystals initially formed in the bulk are still observed. However, after 300 h at 1050 °C, a small proportion of titanite crystals also grows in the bulk at the expense of zirconolite. All, these results were confirmed using both optical absorption and ESR spectroscopies for the Nd-doped GCM. Thus, zirconolite is a metastable phase in the system studied here which contains both titanite and a silica-rich residual glass. Titanite can be considered as the most stable phase incorporating the titanium in this system. However, for kinetic reasons zirconolite is the only crystalline phase which nucleates and grows in the bulk for relatively short crystal growth durations (2 h) at T_c = 1050 °C or 1200 °C. Consequently, in order to reduce the risks of progression of the titanite crystals from the surface towards the bulk of the GCM at the expense of zirconolite, T_c must be not too high and/or the heating duration at this temperature must not exceed a few hours. In these conditions, titanite will remain located in a thin crystallized layer that will probably not affect the long term behavior of the waste form due to the good chemical durability of titanite. Nevertheless, because of the very high kinetic barrier associated with titanite crystal growth during storage and disposal of the GCM, zirconolite would remain kinetically stable and no long-term evolution of both the structure and microstructure of the GCM is expected to occur in these conditions (for minor actinides amounts $\leqslant$10 wt.%, the surface and internal temperatures of the waste forms would never reach values lying in the nucleation and crystal growth ranges).

Acknowledgments

The financial support by the CEA (Commissariat à l'Energie Atomique, France) for this study is gratefully acknowledged. The authors thank C. Fillet (CEA) for fruitful discussions about zirconolite-based GCM.

References

[1] W. Holland, G. Beall (Eds.), Glass–Ceramic Technology, The American Ceramic Society, Westerville, Ohio, 2002.
[2] G.H. Beall, L.R. Pinckney, J. Am. Ceram. Soc. 82 (1999) 5.
[3] G.H. Beall, D.A. Duke, Glass–Ceramic Technology, Glass: Science and Technology, vol. 1, Academic Press Inc., San Diego, 1983, p. 403.
[4] G. Partridge, Glass Technol. 35 (1994) 116.
[5] R.D. Rawlings, J.P. Wu, A.R. Boccaccini, J. Mater. Sci. 41 (2006) 733.
[6] I.W. Donald, B.L. Metcalfe, R.N.J. Taylor, J. Mater. Sci. 32 (1997) 5851.
[7] W.E. Lee, M.I. Ojovan, M.C. Stennett, N.C. Hyatt, Adv. Appl. Ceram. 105 (2006) 3.
[8] M.I. Ojovan, J.M. Juoi, A.R. Boccaccini, W.E. Lee, Mater. Res. Soc. Symp. Proc. 1107 (2008) 245.
[9] D. Caurant, P. Loiseau, O. Majérus, V. Aubin-Chevaldonnet, I. Bardez, A. Quintas, Glasses, Glass–Ceramics and Ceramics for Immobilization of Highly Radioactive Nuclear Wastes, Nova Science Publishers, Hauppauge, New York, 2009.
[10] M.L. Carter, H. Li, Y. Zhang, A.L. Gillen, E.R. Vance, Mater. Res. Soc. Symp. Proc. 1124 (2009) 195.
[11] T.P. O'Holleran, S.G. Johnson, S.M. Frank, M.K. Meyer, M. Noy, E.L. Wood, D.A. Knecht, K. Vinjamuri, B.A. Staples, Mater. Res. Soc. Symp. Proc. 465 (1997) 1251.
[12] A.R. Boccaccini, T. Berthier, S. Seglem, Ceram. Int. 33 (2007) 1231.
[13] P. Loiseau, D. Caurant, N. Baffier, L. Mazerolles, C. Fillet, J. Nucl. Mater. 335 (2004) 14.
[14] D. Caurant, O. Majérus, P. Loiseau, I. Bardez, N. Baffier, J.-L. Dussossoy, J. Nucl. Mater. 354 (2006) 143.
[15] E.R. Vance, A. Jostsons, R.A. Day, C.J. Ball, B.D. Begg, P.J. Angel, Mater. Res. Soc. Symp. Proc. 412 (1996) 41.
[16] E.R. Vance, C.J. Ball, R.A. Day, K.L. Smith, M.G. Blackford, B.D. Begg, P.J. Angel, J. Alloys Compd. 213–214 (1994) 406.
[17] M.C. Stennett, N.C. Hyatt, M. Gilbert, F.R. Livens, E.R. Maddrell, Mater. Res. Soc. Symp. Proc. 1107 (2008) 413.
[18] M.C. Stennett, N.C. Hyatt, D.P. Reid, E.R. Maddrell, N. Peng, C. Jeynes, K.J. Kirkby, J.C. Woicik, Mater. Res. Soc. Symp. Proc. 1124 (2009) 243.
[19] M.C. Stennett, E.R. Maddrell, C.R. Scales, F.R. Livens, M. Gilbert, N.C. Hyatt, Mater. Res. Soc. Symp. Proc. 985 (2007) 145.
[20] C. Guy, F. Audubert, J-E. Lartigue, C. Latrille, T. Advocat, C. Fillet, C.R. Phys. 3 (2002) 827.
[21] C. Fillet, T. Advocat, F. Bart, G. Leturcq, H. Rabiller, C.R. Chimie 7 (2004) 1165.
[22] X. Deschanels, V. Picot, B. Glorieux, F. Jorion, S. Peuget, D. Roudil, C. Jégou, V. Broudic, J.N. Cachia, T. Advocat, C. Den Auwer, C. Fillet, J.P. Coutures, C. Hennig, A. Scheinost, J. Nucl. Mater. 352 (2006) 233.
[23] W.J. Weber, A. Navrotsky, S. Stefanovsky, E.R. Vance, E. Vernaz, MRS Bull. 34 (2009) 46.
[24] A.V. Ochkin, S.V. Stefanosky, A.G. Plashkin, N.S. Mikhailenko, O.I. Kirjanova, Mater. Res. Soc. Symp. Proc. 824 (2004) 267.
[25] F. Jorion, X. Deschanels, T. Advocat, F. Desmoulière, J.N. Cachia, S. Peuget, D. Roudil, G. Leturcq, Nucl. Sci. Eng. 153 (2006) 262.
[26] G.R. Lumpkin, Elements 2 (2006) 365.
[27] K.R. Whittle, K.L. Smith, N.C. Hyatt, G.R. Lumpkin, Mater. Res. Soc. Symp. Proc. 1107 (2008) 331.
[28] D.M. Strachan, R.D. Scheele, E.C. Buck, A.E. Kozelisky, R.L. Sell, R.J. Elovich, W.C. Buchmiller, J. Nucl. Mater. 372 (2008) 16.
[29] A.E. Ringwood, S.E. Kesson, N.G. Ware, W.O. Hibberson, A. Major, Geochem. J. 13 (1979) 141.
[30] P.E. Fielding, T.J. White, J. Mater. Res. 2 (1987) 387.
[31] F. Farges, R.C. Ewing, G.E. Brown, J. Mater. Res. 8 (1993) 1983.
[32] R.C. Ewing, W.J. Weber, W. Lutze, in: E.R. Merz, C.E. Walter (Eds.), Disposal of Weapon Plutonium Approaches and Prospects, Kluwer, Dordrecht, The Netherlands, 1995, p. 65.
[33] W.J. Weber, J.W. Wald, Hj. Matzke, J. Non-Cryst. Solids 138 (1986) 196.
[34] G.R. Lumpkin, R.C. Ewing, B.C. Chakoumalos, R.B. Greegor, F.W. Lytle, E.M. Foltyn, F.W. Clinard, L.A. Boatner, M.M. Abraham, J. Mater. Res. 1 (1986) 564.
[35] J.W. Wald, W.J. Weber, in: G. Wicks, W.A. Ross (Eds.), Advances in Ceramics, Nuclear Waste Management, vol. 8, American Ceramic Society, Columbus, OH, 1984, p. 71.
[36] K.L. Smith, Z. Zhang, P. McGlinn, D. Attard, H. Li, G.R. Lumpkin, M. Colella, T. McLeod, Z. Aly, E. Loi, S. Leung, M. Ridgway, W.J. Weber, S. Thevuthasan, Mater. Res. Soc. Symp. Proc. 757 (2003) 289.
[37] M. Tribet, S. Gavarini, N. Toulhoat, N. Moncoffre, A. Chevarier, C. Jégou, G. Leturcq, C. Corbel, P. Toulhoat, Radiochim. Acta 94 (2006) 585.
[38] M. Tribet, N. Toulhouat, N. Moncoffre, P. Toulhoat, C. Jégou, C. Corbel, I. Bardez, G. Leturcq, Mater. Res. Soc. Symp. Proc. 985 (2007) 335.
[39] G. Leturcq, P.J. McGlinn, C. Barbe, M.G. Blackford, K.S. Finnie, Appl. Geochem. 20 (2005) 899.
[40] T. Wiss, X. Deschanels, J.-P. Hiernaut, D. Roudil, S. Peuget, V.V. Rondinella, J. Nucl. Mater. 362 (2007) 431.
[41] P. Loiseau, D. Caurant, N. Baffier, L. Mazerolles, C. Fillet, Mater. Res. Soc. Symp. Proc. 663 (2001) 179.
[42] P. Loiseau, D. Caurant, O. Majérus, N. Baffier, L. Mazerolles, C. Fillet, Phys. Chem. Glasses 43C (2002) 195.
[43] P. Loiseau, D. Caurant, O. Majérus, N. Baffier, C. Fillet, J. Mater. Sci. 38 (2003) 843.
[44] P. Loiseau, D. Caurant, N. Baffier, C. Fillet, Verre 7 (2001) 8.
[45] D. Caurant, P. Loiseau, I. Bardez, C. Gervais, J. Mater. Sci. 42 (2007) 8558.
[46] P. Loiseau, D. Caurant, O. Majérus, N. Baffier, C. Fillet, Mater. Res. Soc. Symp. Proc. 807 (2003) 333.
[47] D. Caurant, I. Bardez, P. Loiseau, J. Mater. Sci. 42 (2007) 10203.
[48] M. Mahmoudysepehr, V.K. Marghussian, J. Am. Ceram. Soc. 92 (2009) 1540.

[49] T. Advocat, P.J. McGlinn, C. Fillet, G. Leturcq, S. Schuller, A. Bonnetier, K. Hart, Mater. Res. Soc. Symp. Proc. 663 (2001) 277.
[50] C. Martin, I. Ribet, T. Advocat, Mater. Res. Soc. Symp. Proc. 713 (2002) 405.
[51] C. Martin, PhD. Thesis, University of Montpellier II (France), 2002.
[52] P. Frugier, C. Martin, I. Ribet, T. Advocat, S. Gin, J. Nucl. Mater. 346 (2005) 194.
[53] C. Martin, I. Ribet, P. Frugier, S. Gin, J. Nucl. Mater. 366 (2007) 277.
[54] C. Cailleteau, F. Angeli, F. Devreux, S. Gin, J. Jestin, P. Jollivet, O. Spalla, Nat. Mater. 7 (2008) 978.
[55] A. Arab, C. Cailleteau, F. Angeli, F. Devreux, L. Girard, O. Spalla, J. Non-Cryst. Solids 354 (2008) 155.
[56] I. Gutzow, R. Pascova, A. Karananov, J. Schmelzer, J. Mater. Sci. 33 (1998) 5265.
[57] P. Loiseau, D. Caurant, O. Majérus, N. Baffier, C. Fillet, J. Mater. Sci. 38 (2003) 853.
[58] P.J. Hayward, in: W. Lutze, R.C. Ewing (Eds.), Radioactive waste forms for the future, Elsevier Science Publishers, 1988, p. 427.
[59] P.J. Hayward, Glass Technol. 29 (1988) 122.
[60] S. Prowatke, S. Klemme, Geochim. Cosmochim. Acta 69 (2005) 695.
[61] S. Prowatke, S. Klemme, Geochim. Cosmochim. Acta 70 (2006) 4997.
[62] T.H. Green, N.J. Pearson, Chem. Geol. 55 (1986) 105.
[63] M. Tiepolo, R. Oberti, R. Vannucci, Chem. Geol. 191 (2002) 105.
[64] Z. Strnad, Glass–ceramic materials, Glass Science and Technology, vol. 8, Elsevier, 1986, p. 72.
[65] P.W. McMillan, Glass–ceramics, Academic Press, 1979.
[66] V. Maier, G. Müller, J. Am. Ceram. Soc. 70 (1987) C176.
[67] A. Ramos, M. Gandais, J. Cryst. Growth 100 (1990) 471.
[68] P. Riello, P. Canton, N. Comelato, S. Polizzi, M. Vertità, G. Fagherazzi, H. Hofmeister, S. Hopfe, J. Non-Cryst. Solids 288 (2001) 127.
[69] U. Schiffner, in: H. Bach (Ed.), Low Thermal Expansion Glass Ceramics, Springer-Verlag, Berlin Heidelberg, 1995, p. 25.
[70] D. Altermatt, I.D. Brown, Acta Cryst. B41 (1985) 240.
[71] N.E. Brese, M. O'Keeffe, Acta Cryst. B47 (1991) 192.
[72] P. Loiseau, D. Caurant, N. Baffier, C. Fillet, Phys. Chem. Glasses 43C (2002) 201.
[73] K. Gatterer, G. Pucker, W. Jatscher, H.P. Fritzer, S. Arafa, J. Non-Cryst. Solids 231 (1998) 189.
[74] A.F. Wells, Structural Inorganic Chemistry, Oxford University Press, 1962. p. 808.
[75] W.A. Deer, R.A. Howie, J. Zussman, Rock-Forming Minerals, Framework Silicates, vol. 4, John Wiley & Sons, New York, 1963.
[76] H. Müller, in: H. Bach, D. Krause (Eds.), Analysis of the Composition and Structure of Glass and Glass Ceramics, Springer, 1999, p. 52.
[77] W.L. Gong, W. Lutze, R.C. Ewing, J. Nucl. Mater. 277 (2000) 23.
[78] J.M. Hughes, E.S. Bloodaxe, J.M. Hanchar, E.E. Foord, Am. Min. 82 (1997) 512.
[79] J.H. Higgins, P.H. Ribbe, Am. Min. 61 (1976) 878.
[80] E.R. Vance, D.K. Agrawal, Nucl. Chem. Waste Manage. 3 (1982) 229.
[81] P. Duwez, E. Loh, J. Am. Ceram. Soc. 40 (1957) 321.
[82] R.D. Shannon, Acta Cryst. A32 (1976) 751.
[83] O.V. Mazurin, G.P. Roskava, E.A. Porai-Koshits, Phase Separation in Glasses, Elsevier, 1984. p. 108.
[84] L. Pauling, J. Am. Chem. Soc. 51 (1929) 1010.
[85] G.E. Brown, F. Farges, G. Calas, Rev. Min. 32 (1995) 317.
[86] F. Angeli, D. Boscarino, S. Gin, G. Della Mea, B. Boizot, J.C. Petit, Phys. Chem. Glasses (2001) 279.
[87] L. Trotignon, J.C. Petit, G. Della Mea, J.C. Dran, J. Nucl. Mater. 190 (1992) 228.
[88] A. Paul, Chemistry of Glasses, Chapman and Hall, 1990. p. 179.
[89] A. Duddridge, M. Islam, D. Holland, C.R. Scales, Mater. Res. Soc. Symp. Proc. 807 (2004) 145.
[90] International Center of Diffraction Data Base (ICDD), release 2007.
[91] A. Quintas, O. Majérus, D. Caurant, J.-L. Dussossoy, P. Vermaut, J. Am. Ceram. Soc. 90 (2007) 712.
[92] G.J. McCarthy, J.G. Pepin, D.E. Pfoertsch, D.R. Clarke, Ceramics in nuclear waste management, in: T.D. Chikalla, J.E. Mendel, (Eds.), Proceedings of an International Symposium, Cincinnati, 1979, p. 315.
[93] F.P. Glasser, Br. Ceram. Trans. J. 84 (1985) 1.
[94] J.W. Wald, W.J. Weber, Nuclear waste management, in: G.G. Wicks, W.A. Ross (Eds.), Advances in Ceramics, vol. 8, American Ceramic Society, Inc., Columbus, OH, 1984, p. 71.
[95] P. Loiseau, PhD Thesis, University Paris VI, France, 2001.
[96] R. Guillaumont, C.R. Chimie 7 (2004) 1129.